Design and Development of a Two-Axis Reluctance Based Actuator
for Hexflex Nano-Positioner

by

Howard J. Liles
Submitted to the Department of Mechanical Engineering
in Partial Fulfillment of the Requirements for the
Degree of
Bachelor of Science in Mechanical Engineering

at the

Massachusetts Institute of Technology

June 2010

Signature of Author.....
Department of Mechanical Engineering
May 14, 2010

Certified by.....
Martin L. Culpepper
Associate Professor of Mechanical Engineering
Thesis Supervisor

Accepted by.....
John H. Lienhard V
Collins Professor of Mechanical Engineering;
Chairman, Undergraduate Thesis Committee

Design and Development of Two-Axis Reluctance Based Actuator

for Hexflex Nano-Positioner

by

Howard J. Liles

Submitted to the Department of Mechanical Engineering
on May 14, 2010 in Partial Fulfillment of the
Requirements for the Degree of Bachelor of Science in
Mechanical Engineering

ABSTRACT

An endeavor was conducted to explore the design and development of a two-axis linear reluctance actuator for use as a part of a nano-positioner with the application of serving as a small scale kinematic coupling assembly station. This nano-positioner is designed to be able to accurately and repeatable provide precise motion control of small objects with a resolution on the nanometer scale. This device uses a novel monolithic flexure (Hexflex) that enables it be repeatable to a few nanometers and also very inexpensive to manufacture. The reluctance actuator will provide the force necessary to actuate the positioning system. This actuator type was compared to other actuator types to verify its feasibility and relevance for this application. The actuator operates based off of the reluctance principle used in magnetic circuits and its application as a two-axis actuator is a new and unexplored technology. It will be designed using solid modeling software and magnetic circuit theory, constructed, and tested as a part of the thesis project. Several design iterations were conducted yielding valuable design, manufacturing, and assembly knowledge and insight. Ultimately the actuator did not function properly and consequently did not meet the performance criterion necessary to be incorporated into the nano-positioner system. Due to a correlation disparity between the governing model and the manufactured device, the actuator did not function as predicted and was unusable. Furthermore, after efforts to remedy the problems, the conclusion was reached that the necessary changes would result in the use of this actuator being unfeasible for this application. However, the insight and designs produced from this research has the potential to aid in the further development of this reluctance actuator technology.

Thesis Supervisor: Martin L. Culpepper
Title: Associate Professor of Mechanical Engineering

ACKNOWLEDGEMENTS

To my advisor, Prof Martin Culpepper, thank you for allowing me to participate in your research. Thanks so much for all the support and guidance that you have provided me as I completed this project.

I would like to thank Robert Panas for his support and assistance in the magnetic theory and conceptualization of this project. His help and ideas were invaluable to the generation of this device.

I would also like to thank the researchers in Professor Culpepper's Lab, the Precision Compliant Systems Laboratory (PCSL) and the staff of the Lab for Manufacturing and Productivity (LMP) for their friendly help and advice concerning the manufacturing of the components of my project.

Finally, I would like to thank the MIT Department of Mechanical Engineering for the excellent instruction, opportunities, and experiences that it has provided me during my time at MIT.

CONTENTS

FIGURES

TABLES

CHAPTER

1

INTRODUCTION

1.1 Purpose

The purpose of this research is to explore in detail, the design and development of a two-axis reluctance based actuator shown in Figure 1.1. A new technology was explored utilizing tangential reluctance forces generated by a magnetic coil to assist in nano-scale manipulation. Over a specific range, these devices have the potential to provide a high force, low cost precision actuator to the emerging micro and nano-scale manufacturing fields.

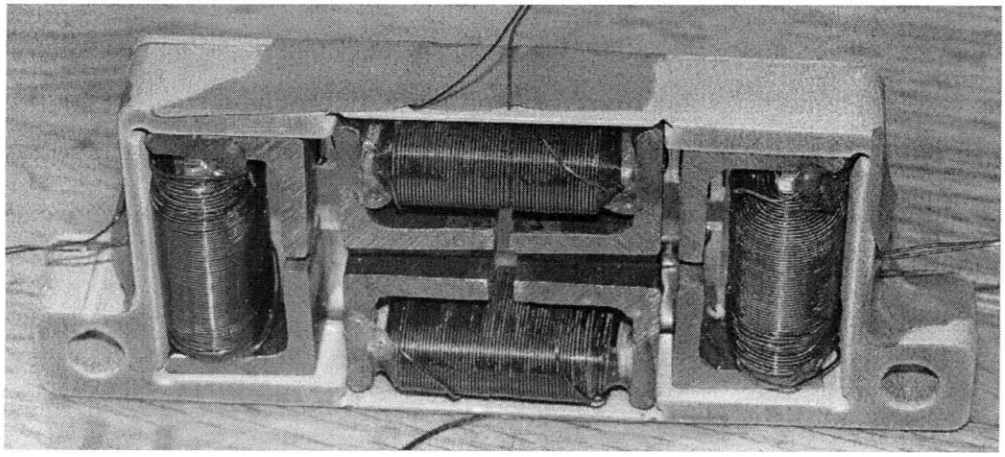

Figure 1.1: Reluctance actuator prototype

This thesis will also discuss the actuator selection process, design requirements, the design process, and the manufacturing process of the actuators. The knowledge and insight obtained in the investigation of this class of actuators will provide future researchers and scientists with an increased capability to develop and produce actuators and apply them to nano-scale technology.

1.2 Motivation

Nano-scale devices open the door for many technologies and innovations. Creating devices and trying to work on this scale has proven to be quite a difficult task. Applications such as fiber optic aligners and manufacturing of small components such as kinematic couplings for nano-scale devices require ultra precise manipulators which are often very expensive ($15,000 - $100,000) [1]. Furthermore, due to the fact that the devices are so small, it is difficult to manufacture them to the necessary precision and tolerances. The high cost of these manipulators acts as a limiting factor for the commercial feasibility of these new small scale technologies and innovations. Thus, there is a need for precision positioning equipment that exhibits high cost-performance characteristics in order for these new and emerging technologies to fully develop and reach their potential. An essential quality of any new equipment will be its ability to accurately and repeatedly actuate and position pieces with a nano-scale resolution.

The Hexflex is a monolithic, positioning stage utilizing a six axis compliant mechanism that possess this quality [1]. A Hexflex is shown in Figure 1.2. It has demonstrated the ability to effectively position its stage with a resolution below 5nm. To fully take advantage of this new device, actuators must be developed that are capable of applying the necessary forces and comparable resolution, accuracy and repeatability. Furthermore they must be able to do so in a timely manner and be capable of being manufactured in a cost effective manner. This will enable industry to further utilize nano-scale devices and take advantage of the unique capabilities that this technology provides.

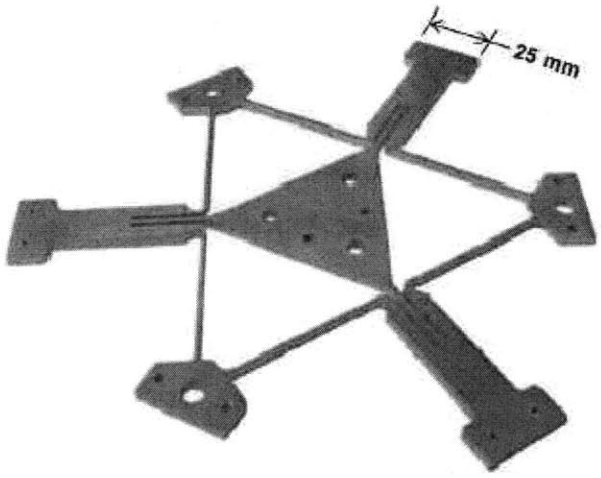

Figure 1.2: Hexflex flexural positioning stage [1]

More particularly, this research project will explore actuation technology to develop a device that is ideal for aiding in nano-scale manipulation particular for the application of manufacturing small-scale kinematic couplings. The actuator, along with the Hexflex and an optical vision control system, will be incorporated into an assembly station capable of producing these devices.

1.3 Hexflex Flexural Positioning Stage

The Hexflex nano-positioner is a monolithic precision manipulator that accurately and repeatedly positions its stage with a resolution greater than 5nm over a work rang of 100μm × 100μm × 100μm and open-loop parasitic errors less than 5mm. The device exhibits lower thermal drift in its position and orientation (less than 23nm and 4μrad over a 30 min start-up period. The Hexflex utilizes a compliant mechanism and equilateral geometric design to achieve this accuracy and stability [1]. It has the capability of six-axis movement due to its novel design. Not only is this device accurate, but it may also be manufactured for $2000 (excluding electronics).

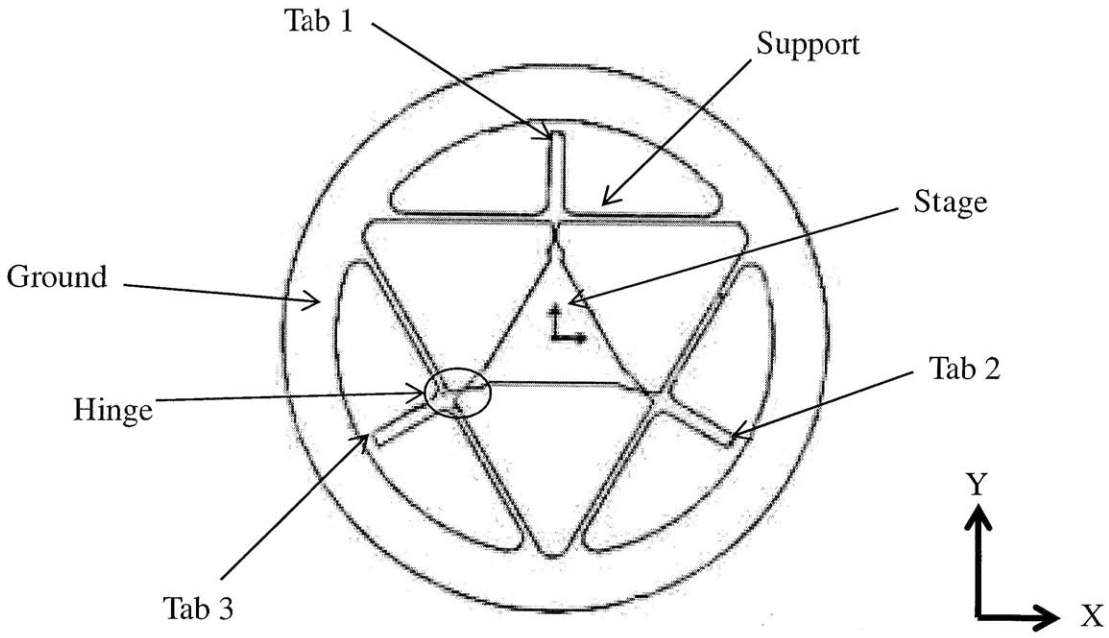

Figure 1.3: Hexflex component description [1]

As can be seen in Figure 1.3, the Hexflex has three lever arms, or tabs, which are actuated to provide the desired motion to the stage. Figure 1.4 illustrates how various combinations of forces on the tabs yeild its six axis mobility. The forces on a tab create reaction forces and reaction moments in the center stage. Each individual tab may be actuated in-,and out-of-plane. Consequently each tab needs actuation in two dimensions to induce the 6-axis capabilities of the Hexflex.

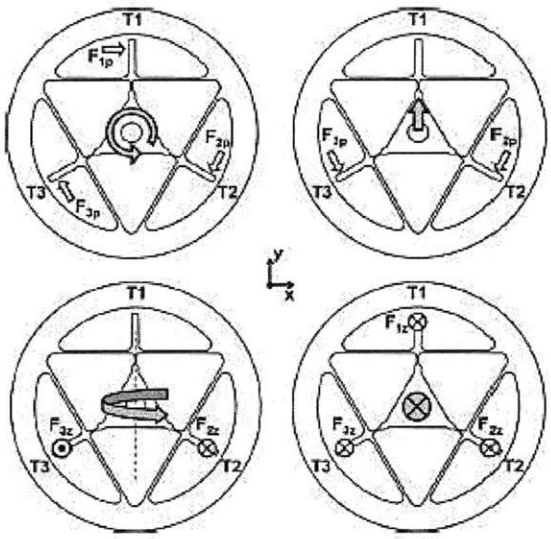

Figure 1.4: Force combinations for Hexflex stage manipulation [1]

This nano-positioner is integrated with electronics and actuators to form a complete system. A concept model for this system may be seen in Figure 1.5. As shown in the figure, the system has three actuators to control the three tabs of the Hexflex. This model includes the Hexflex, actuators, and all other mechanical components that form the manipulator. The electronics and vision system are not shown in the figure.

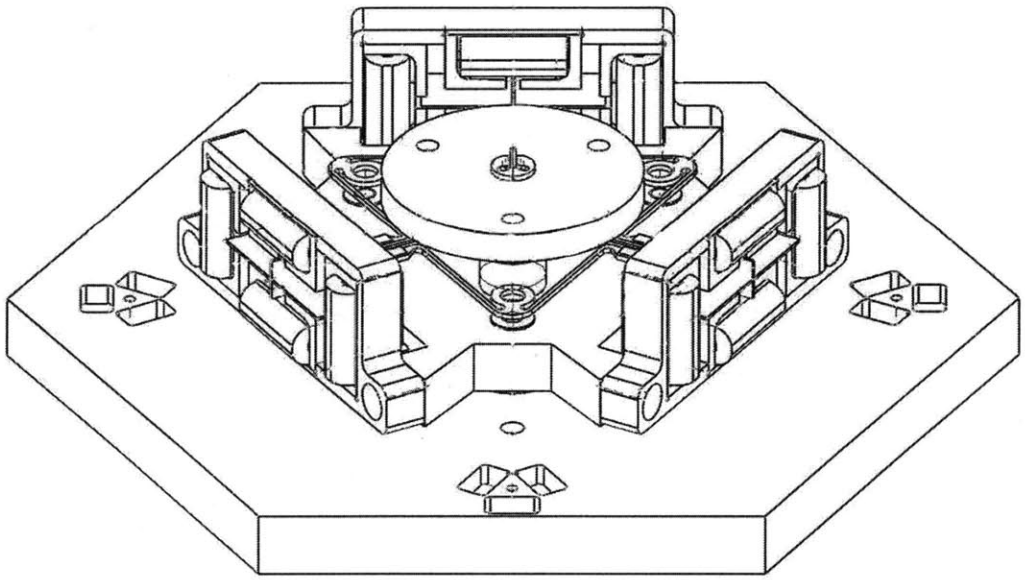

Figure 1.5: Complete nano-positioning system with Hexflex and reluctance actuators

The actuators for this system require comparable performance characteristics and low-cost for the entire nano-positioning system to be practical. Several precision were investigated: piezo-electric, voice coil, and reluctance actuators. After researching the various actuators, the reluctance actuator was selected and development of this concept continued. This actuated demonstrated the potential to yield high output forces when compared with other actuators used for small scale actuation. It also possessed a relatively simple design and low manufacturing cost (~$100).

CHAPTER 2 BACKGROUND

2.1 Magnetic Circuits

Reluctance based actuators operate off of the reluctance principle observed in magnetic circuits. Due to this phenomenon, these actuators are able to produce forces while remaining relatively small in size. To better understand how this device, a little background on magnetic circuits is required.

Maxwell's Equations are the primary governing equations for the scenarios that will be discussed. Ampere's Law, Gauss's Law for Magnetism and Faraday's Law are the primary operators. They will enable us to effectively relate magnetic fields to current. For simplicity, Ampere's Law and Gauss's Law will be discussed alone and then the application of Faradays law will be discussed afterward.

In using these equations, it is assumed that there are no time varying electric fields. By making this assumption, a magneto-quasistatic form of Maxwell's equations is produced.

Equation 2.1 is Ampere's Law. It states that the line integral of the tangential component of **H** (the Magnetic Field intensity) around a closed contour, C, is equal to the total current passing through any surface, S, connecting that contour. Therefore, in this equation, the magnetic field intensity is caused by the current density, J [3].

Equation 2.2 is Gauss's Law for Magnetism. It states that the magnetic flux density, $\boldsymbol{B}$ is conserved. This means that there is no net flux entering or leaving a closed surface, that no magnetic monopoles exist.

$$\oint_C \boldsymbol{Hdl} = \int_S \boldsymbol{J} \cdot \boldsymbol{da} \tag{2.1}$$

$$\oint_S \boldsymbol{B} \cdot \boldsymbol{da} = 0 \tag{2.2}$$

Consequently the magnetic flux, φ, entering a closed surface must equal the magnetic flux leaving that same closed surface. This magnetic flux is also equal to the surface integral of the normal component of the magnetic flux density, $\boldsymbol{B}$

$$\varphi = \oint_S B \cdot da \tag{2.3}$$

and this relation can be further simplified to a scalar equation when the magnetic flux density is uniform across the cross sectional area, A_C, through which it is flowing. This holds true for the analysis being conducted :

$$\varphi = BA_C \tag{2.4}$$

Using these equations to determine magnetic field intensity and magnetic flux intensity within a complex three-dimensional is difficult. The use of a magnetic circuit analogy will simplify the necessary calculations. The magnetic circuit analogy assumes the use of materials that have a high magnetic permeability so that magnetic flux is mostly confined within the path defined by the material. Figure 2.1 illustrates this analogy. In the figure, current flowing through the coil

windings induces a magnetic flux to flow within the magnetic core of material. This current carrying coil generates what is commonly known as a magnetomotive force, $\mathcal{F}$, within the magnetic circuit. This force is directly dependent on the amount of current, i, flowing through the coil and the number of turns, N, in the coil.

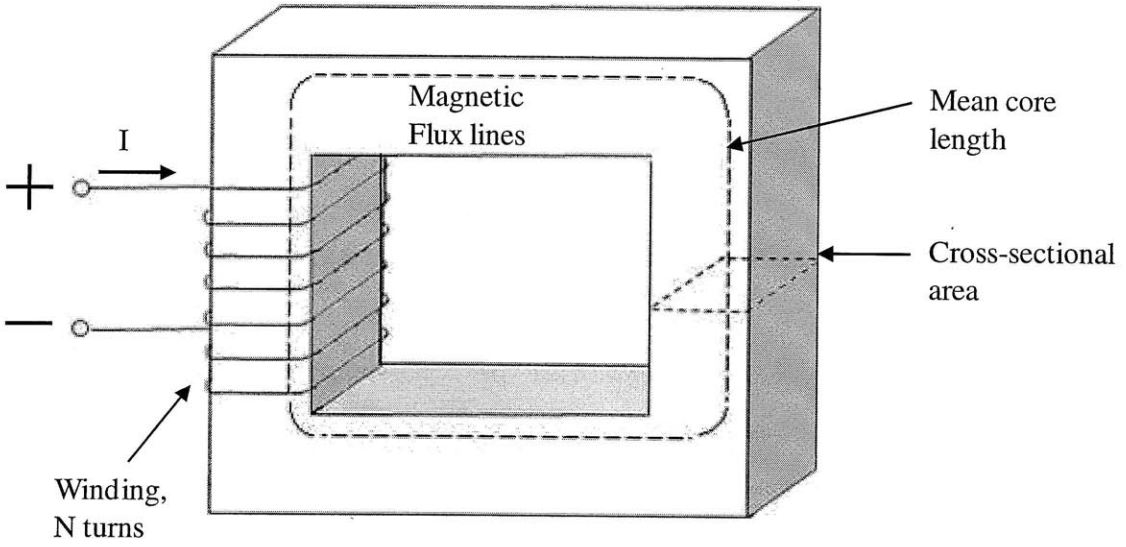

Figure 2.1: Magnetic circuit consisting of coil winding and highly magnetically permeable core [3]

Using the preceding definition and Equation 2.1, we may establish a relationship between, $\mathcal{F}$, and the magnetic field intensity:

$$\mathcal{F} = Ni = \oint \boldsymbol{Hdl} \qquad 2.5$$

Given the dimensions of the core used in our analysis, displayed in Figure 2.1, any line of magnetic flux will be approximately the same as the average core length l_c. Thus the line integral in Equation 2.3 may be further simplified to a scalar multiplication yielding:

$$\mathcal{F} = Ni = H_c l_c \qquad 2.6$$

With H_c representing the average magnitude of the magnetic field intensity within the core.

The magnetic field intensity is commonly assumed to be linearly proportional to the magnetic flux density and is related via a constant known as the magnetic permeability, μ, yielding the following:

2.7

With these relations we construct a model magnetic circuit which can be used to explain the key factors that dominate a reluctance actuator's performance. Figure 2.2 introduces an air gap into the magnetic circuit.

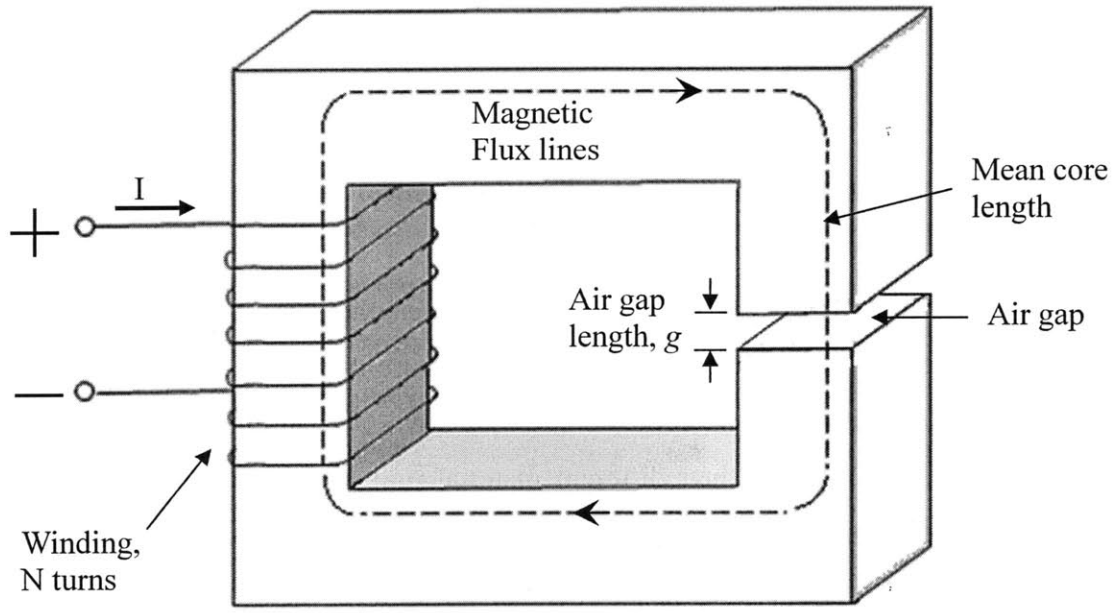

Figure 2.2: Magnetic circuit with air gap introduced into core [3]

When this gap is much smaller than the dimensions of the neighboring pieces (length and width of the cross sectional area of the core above and below the air gap), the magnetic flux will follow the same path as in Figure 2.1. Air has a much lower magnetic permeability than the magnetic core. If the height of this gap becomes too large, then the flux will not exactly follow this predefined path, and no longer be confined to the geometry of the core. Figure 2.3 illustrates this phenomenon. Consequently this air gap must remain relatively small in comparison to the other core dimensions in order for the magnetic circuit analogy to be accurate.

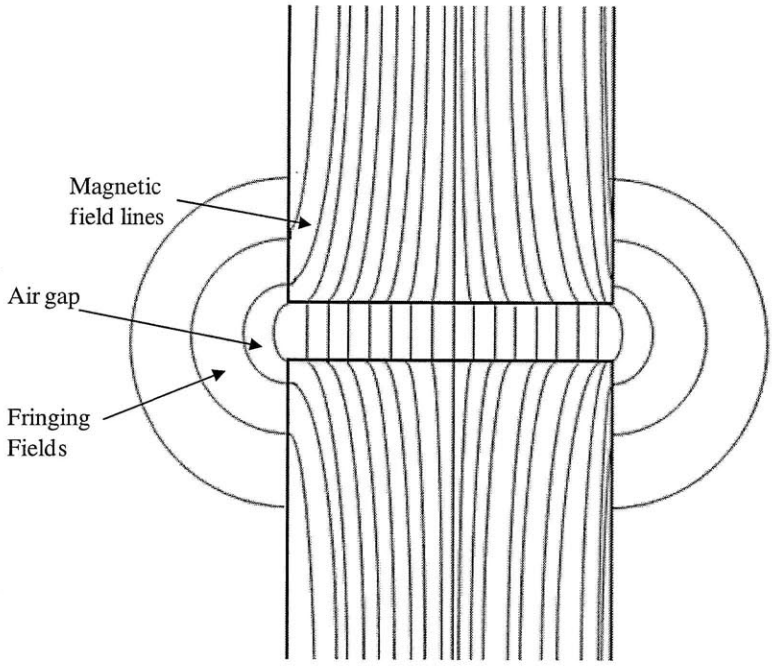

Figure 2.3: Magnetic field lines traveling through core and air gap [3]

Using Equations 2.4, 2.6, 2.7 we develop a relation between the magnetomotive force, the magnetic properties and flux density of the core shown in Figure 2.2, and its geometry. Special care must be taken to differentiate between the core (denoted with a C subscript) and the air gap (denoted with a g subscript) due to their different material properties. Equations 2.8 and 2.9 correspond to the core and air gap respectively. Furthermore, Equation 2.10 shows the summation of $\mathcal{F}$ due to the core and air gap. Equation 2.7 is then used to obtain the second relation of Equation 2.10.

$$B_C = \frac{\varphi}{A_C} \tag{2.8}$$

$$B_g = \frac{\varphi}{A_g} \tag{2.9}$$

$$\mathcal{F} = H_c l_c + H_g g \qquad 2.10$$

$$= \frac{B_c}{\mu_c} l_c + \frac{B_g}{\mu_g} g$$

After some algebraic manipulation and combining of equations, a form similar to Ohm's Law, is obtained:

$$\mathcal{F} = \varphi \left(\frac{l_c}{A_c \mu_c} + \frac{g}{A_g \mu_g} \right) \qquad 2.11$$

The magnetomotive force is analogous to voltage; the magnetic flux is analogous to the current; and the two terms in the parenthesis are the reluctance of the core and the reluctance of the air gap which correspond to resistances in the electric circuit model. Thus the strategies and techniques used in evaluating electric circuits are also applicable here. The core with the air gap is modeled using as an electric circuit with a voltage sources and two resistors in series as shown in Figure 2.4. Now the total reluctance of the circuit may be calculated. This will be important in determining the path along which the magnetic field lines travel to form the desired magnetic circuit.

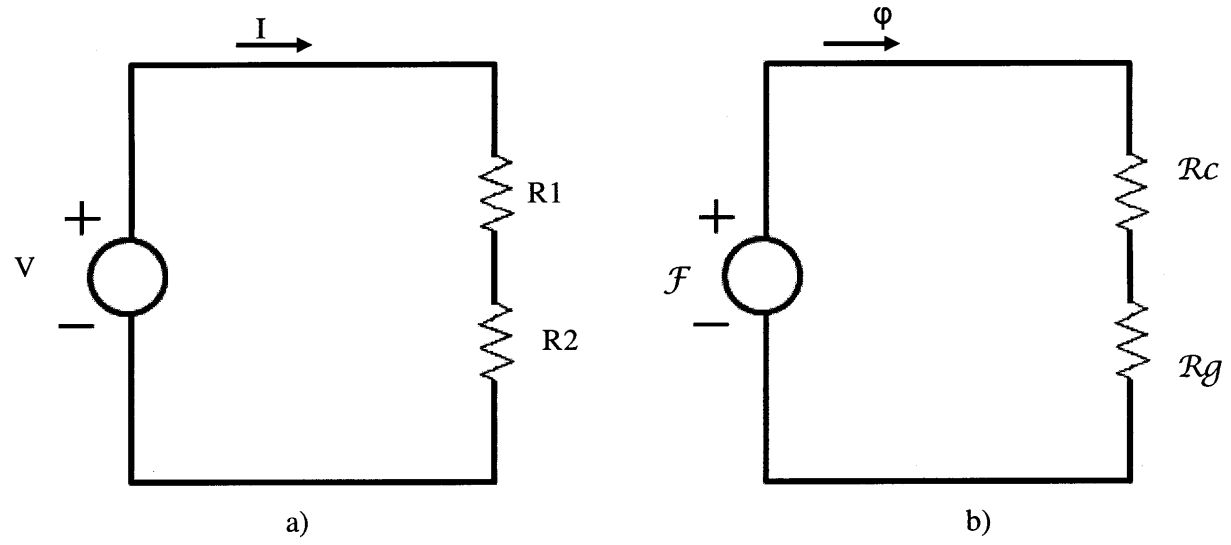

Figure 2.4: Magnetic circuit/electric circuit analogy diagram [3]

Faradays law describes the effects of a magnetic field that varies with time:

$$\oint_C \boldsymbol{E} \cdot \boldsymbol{ds} = -\frac{d}{dt}\int_S \boldsymbol{B} \cdot \boldsymbol{da} \qquad 2.12$$

It states that the line integral of electric field intensity, $\boldsymbol{E}$, around a closed contour, C, is equal to the time rate of change of the magnetic flux which passes through that contour. In the analysis of devices with highly conductive windings, e.g. the copper coil wound around one end of the core, the $\boldsymbol{E}$ field in the wire is neglected as it is generally small. The magnetic flux flowing through the closed contour is dominated by the flux flowing through the magnetic core. Thus, Equation 2.12 simplifies to:

$$e = N\frac{d\varphi}{dt} = \frac{d\lambda}{dt} \qquad 2.13$$

in which the flux linkage, λ, represents the product of the number of turns in the coil and the magnetic flux. This equation states that the magnitude of the electromotive force, e, is proportional to the rate of change of magnetic flux. In our application, we use a magnetic core composed of material with a constant magnetic permeability. Performance is dominated by the reluctance of the air gap. The flux linkage is linearly related to the current flowing through the wire by its inductance:

$$L = \frac{\lambda}{i} \qquad 2.14$$

After replacing the sum of the reluctance terms with R_{total}, we substitute this equation, equations 2.5, 2.11, and the definition of the flux linkage to obtain the relation:

$$L = \frac{N^2}{R_{total}} \qquad 2.15$$

This relation shows the inductance of a magnetic coil is proportional to the square of the number of turns in the coil and is inversely proportional to the total reluctance. It is noteworthy that the concept of inductance only applies when a linear relationship between flux and magnetomotive

force exists. If the nonlinear characteristics of magnetic materials dominate the system's performance, then the inductance concept and thus equations 2.14 and 2.15 are no longer valid.

2.2 Material Properties

As a material with a high magnetic permeability is needed to properly direct the magnetic fields within them, ferromagnetic materials are used to construct the core and plunger of the actuator. These ferromagnetic materials are composed of alloys of iron with cobalt, tungsten, nickel, and aluminum. Care must be taken with the use of these materials because of the magnetic field lines' tendency to follow the path of least resistance, the magnetic steel should only be used in constructing the core and components through which it is desirable to have a flow of magnetic flux. Using highly magnetically permeable material as a part of the actuator's structure or other components could potential redirect the magnetic field lines along an undesired path and result in a non-functional actuator.

Ferromagnetic materials contain a large number of magnetic domains, i.e. regions in which the atoms exhibit magnetic moments that line up in parallel manner and create a net magnetic moment for the region. When the material is not magnetized, these domains are randomly oriented and cancel each other out. When an external magnetizing force is applied to the material, these domains line up with that magnetic field, and add to it, yielding an increase in the field's flux density. Consequently, it is desirable to select an iron or alloy possessing a low carbon content since carbon acts as an impurity and does not exhibit the necessary magnetic behavior [4]. Using iron with low carbon contents will maximizes the magnetic properties of the parts.

2.3 Saturation

There are also other noteworthy factors that limit the performance of this device. Magnetic forces and energy densities increase as the magnetic flux density flowing through a given core increase. There is a limit to the amount of magnetic flux that may flow through the magnetically permeable material. When all the magnetic domains have lined up with the external magnetic force, the material is said to be saturated and no more gains in field flux density may be achieved. Initially the flux increases proportionally to the applied magnetic field, however, it

soon begins to level off as most of the domains align resulting in smaller and smaller increases in magnetic flux density as the applied field increases. Saturation begins to occur when the ratio of magnetic flux to the cross sectional area of the magnetic material reaches about 1.

2.4 Reluctance Actuation

Reluctance based actuators are electromechanical devices that convert electrical work into mechanical work. In these devices the electrical energy actually changes form and is stored within magnetic field of the device. These actuators take on various forms; however, this discussion will explore a linear actuator which looks very similar to the magnetic circuit pictured in Figure 2.5.

The basic principle is that the magnetic field lines traveling through the magnetic core always desire to travel the path of least reluctance, or "resistance" when applied to our electric circuit analogy. As the air gap has a much lower magnetic permeability, it has a high reluctance. If the gap is too large, the reluctance may be so large that the magnetic field lines are not able to jump the gap and an open circuit occurs. If a piece of material with a high magnetic permeability is placed within the air gap, the total distance of air that the magnetic field lines must travel is decreased. This results in the magnetic field lines jumping the shorter air gap, flowing easily through the magnetically permeable material and then jumping the other small air gap back into the magnetic core. Figure 2.5 illustrates this set up.

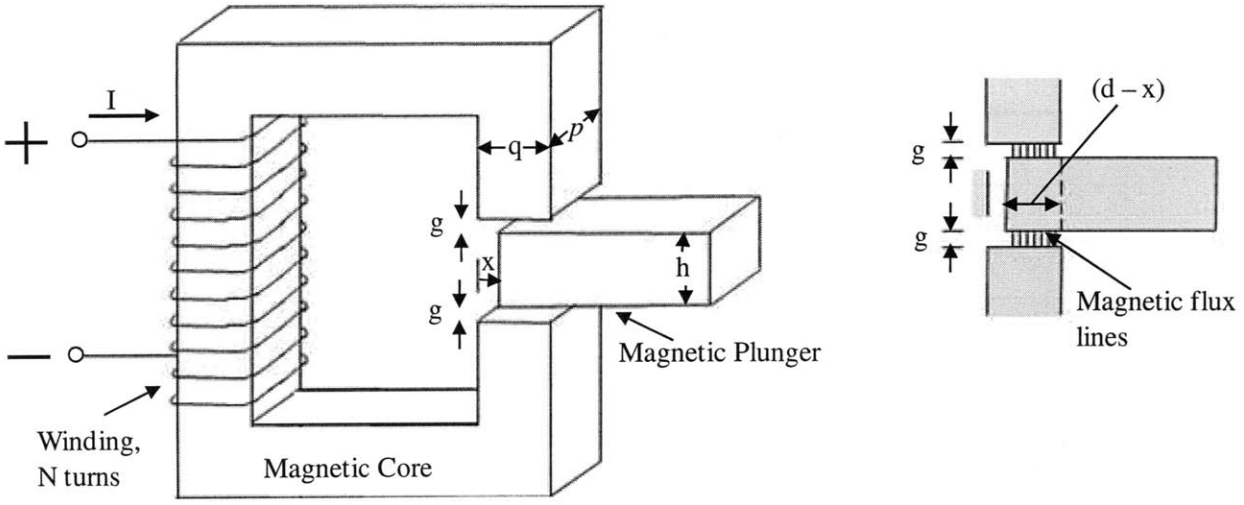

Figure 2.5: Magnetic circuit set-up for modeling actuator [3]

One can imagine the magnetic flux path to be a column with sides defined by the dimensions of the arms of the magnetic core and extending across the air gap. Due to the fact that the magnetic field lines want to travel the path of least resistance, they will exert a force on the magnetically permeable material, which will be referred to as a plunger, until it completely crosses the column and minimizes the amount of air within the column. It is this force that is taken advantage of by the linear actuator to accomplish its task.

CHAPTER

3

DESIGN REQUIREMENTS

3.1 Actuator Requirements

In order for an actuator to function properly as part of the Hexflex system, it is necessary for certain design requirements to be fulfilled. These requirements are vital in order for the system to

perform at an acceptable level. Table 3.1 displays some of the design requirements considered in this project.

Table 3.1: Summary of actuator critical requirements	
Cost To manufacture	≤$1500
Force	≥5N
Range	≥1.25mm
Resolution	≤50nm

3.1.1 Cost

The nano-manipulator system must be relatively inexpensive in order to justify its use. The actuator must be of lower or comparable cost with the other components of the system in order for it to be a suitable candidate. The cost of the actuator includes it material costs, manufacturing costs, and any associate maintenance costs.

3.1.2 Force

An actuator must be able to generate an appropriate amount of force to move and manipulate the Hexflex tabs. The minimum requirement for this force is approximately 5N.

3.1.3 Range

The actuator must have sufficient stroke length to effectively manipulate the Hexflex over a desired range. If this range is too small then, the work volume that the entire system will be limited. The minimum requirement for this parameter is approximately 1.25mm.

3.1.4 Resolution

In order for the device to be able to manipulate objects on the nanometer scale it must have sufficient resolution to move objects at that length scale. Without this characteristic the manipulator will be virtually useless for small scale operations. The resolution requirement for this actuator is approximately 50 nanometers.

3.1.5 Thermal Response

When the actuator is powered, it will produce heat and this heat must be dissipated to prevent the actuator from overheating. Furthermore, the heat must be dissipated away from the Hexflex because an increase in temperature will result in thermal errors. These errors are undesirable and may affect the accuracy of the device Consequently the actuator must be able to quickly and effectively dissipate any heat that it generates.

3.1.6 Complexity/Compatibility with Hexflex

The actuation device must also be easily integrated with the flexure. Simplicity and a low part count are also advantageous because they decrease the potential for error and reduce the potential number of parts that must be replaced. These qualities can also decrease maintenance costs and setup and operation time. Easy integration with the flexure is crucial in order to maintain accuracy, response time, and reduce the need for additional components.

3.1.7 Response Rate/Disturbance Response

A low response time is a desirable to decrease the amount of time it takes to actuate the Hexflex and yield a high productivity for the system. It is also desirable for the actuator to be very stiff so as to have a low response to unwanted environmental disturbances. Ultimately, it is desirable to maximize the stiffness of the actuator.

CHAPTER 4

ACTUATOR TECHNOLOGY

4.1 Actuator Selection

This research is characterized by a lower force need but an increased need for accuracy and resolution. Three of the most common, small-scale actuators were investigated for use with the Hexflex: voice coil, piezoelectric, and reluctance.

4.1.1 Piezoelectric

Piezoelectric materials are a class of crystals that do not have a center of symmetry and undergo a dimensional change when an electric potential gradient or electric field is applied to them. This dimensional change is directly proportional to the electric field that is applied to it. These actuators are capable of sub-nanometer resolution, very short response times, and can generate significant forces. It is typically limited to a range of 0-200μm [2].

4.1.2 Voice Coil

Figure 4.1 illustrates the general principle that these devices utilize. A permanent magnetic generates a magnetic field within in a small air gap. A conducting coil is positioned within this air gap. When current is sent through the coil, it generates a magnetic field which interacts with the magnetic field created by the magnetic. This interaction results in an axial force between the core and the coil along their common axis. The force created is proportional to the strength of the magnet and the gradient of the field perpendicular to the axis of its poles.

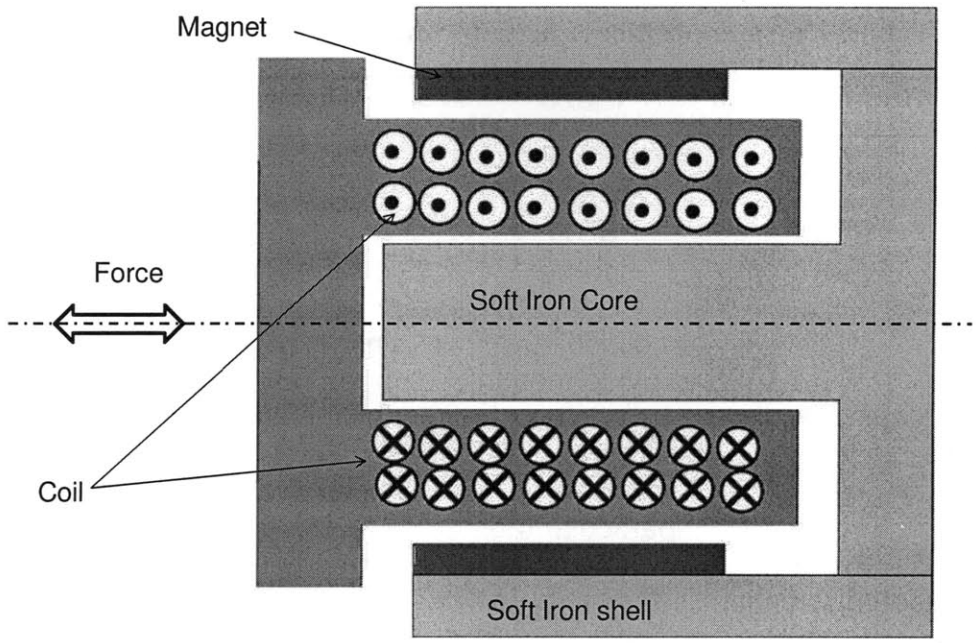

Figure 4.1: Cross sectional side view of voice coil

This force requires a balancing force which is often provided by a spring or sometimes another voice coil acting in the opposing direction. The opposing springs are actually the limiting factor in the accuracy of the actuator. When using a spring created from a single-crystal piece of silicon open loop displacements of 100nm with a resolution of 5pm may be achieved. For a completely saturated magnet in a relatively weak field, the force/current characteristic has been found to be linear to within better than one part in 10,000 [5].

4.1.3 Reluctance Actuators

The premise of reluctance actuators are described in detail in Chapter 2. As shown in Table 4.1, these actuators exhibit significant force capabilities, simple design, and significant range.

4.1.4 Selection

A Pugh chart was utilized to systematically compare and objectively rank the actuators based on their various capabilities. Table 4.1 shows the criterion used within this pugh chart and describes the characteristics of the various actuators.

Table 4.1: Nano-positioner actuator pugh chart criterion [2],[3],[6]

Functional Requirements	Piezo	Reluctance	Voice Coil
Force	Kilo-Newton	500-1250N	50N
Range	80μm	1250μm	500μm
Cost	$700	~$100	<$500
Resolution	sub-nm	1 nm RMS	open loop as low as .01nm
Complexity	difficult to provide motion along two perpendicular axis for a particular tab	simple, requires plunger, no physical connection necessary, capable of motion along two axis	simple, no physical connection necessary, capable of motion in two perpendicular axis
Heat generation/dissipation	milliwatts	10 times better than voice coil	poor but countermeasures exist

The pugh chart shown in Table 4.2 displays the comparison of characteristics. The piezoelectric actuator was chosen as the baseline actuator to which the other two were compared.

Table 4.2: Nano-positioner actuator pugh chart

Functional Requirements	Piezo	Reluctance	Voice Coil
Force	0	0	-
Range	0	+	+
Cost	0	+	+
Resolution	0	0	0
Complexity	0	+	+
Heat generation/dissipation	0	-	-
Total	0	2	1

This chart aided in determining which actuator was most suitable for this application. A reluctance based actuator was chosen as the ideal candidate for this project due to its simplicity, high output force, and low cost.

CHAPTER

5

ACTUATOR MODEL AND DESIGN

5.1 Governing Model

The theoretical model used to design the actuator is based on the magnetic circuit principles discussed in Chapter 2. Energy is primarily stored within the air gap due to the fact that its reluctance is much higher than that of the magnetically permeable core. Consequently the dimensions of this air gap are the main controlling factors of the performance and properties of the magnetic circuit. As discussed earlier, magnetic nonlinearities are neglected due to their small role in the circuit. Thus the model operates under the assumptions that the magnetic flux and magnetomotive force are directly proportional for the circuit; and the flux linkage, λ, and the current, i, are related in a linear manner via the inductance. The inductance is completely dependent on the geometry and plunger position denoted as x:

$$\lambda = L(x)i \tag{5.1}$$

The forces generated by this actuator may be calculated using a form of conservation of energy, the principle of virtual work:

$$dW_{elec} = dW_{mech} + dW_{field} \tag{5.2}$$

where dW_{elec} is the electrical energy input into the system, dW_{mech} is the mechanical energy or work output from the system, and $dW_{field}$is the change in energy stored within the magnetic field. Energy loss through heat dissipation would also occur and could be a term on the right side of Equation 5.2; however, we are creating a basic idealized model assuming the heat dissipation

to be negligible, and thus it is ignored for now. The magnetic force acting on the plunger is denoted as f_{field}. This force does work, denoted dW_{mech}:

$$dW_{mech} = f_{field}dx \tag{5.3}$$

dW_{elec} may also be written as the product of voltage and current:

$$dW_{elec} = ei\,dt \tag{5.4}$$

Furthermore, by referring back to Equation 2.13, $dW_{elec} = id\lambda$ and when substituted into Equation 5.2:

$$dW_{field} = id\lambda - f_{field}dx \tag{5.5}$$

Due to the fact that we are assuming a lossless, ideal scenario; and as dW_{field} is uniquely dictated by λ and x; these variables are classified as state variables and their values determine the state of the system. Since W_{field} is uniquely determined by the value of λ and x, W_{field} may be integrated in a path independent manner. This makes evaluating Equation 5.5 easier:

$$W_{field}(\lambda_0, x_0) = \int_0^{\lambda_0} i(\lambda, x_0)d\lambda \tag{5.6}$$

As our system is linear and proportional to the current, i, Equation 5.6 yields:

$$W_{field}(\lambda, x) = \int_0^{\lambda} i(\acute{\lambda}, x)d\acute{\lambda} = \int_0^{\lambda} \frac{\acute{\lambda}}{L(x)}d\acute{\lambda} = \frac{1}{2}\frac{\lambda^2}{L(x)} \tag{5.7}$$

Also due to the fact that Equation 5.7 is a state function, we know that for any state function of two independent variables the total differential of the function with respect to the two variables may be written:

$$dW_{field}(\lambda, x) = \frac{\partial W_{field}}{\partial \lambda}\Big|_x d\lambda + \frac{\partial W_{field}}{dx}\Big|_\lambda dx \tag{5.8}$$

As λ and x are independent variables, Equations 5.7 and Equation 5.8 must be true for all values of dλ and dx thus i and f_{field} may be substituted

$$i = \frac{\partial W_{field}(\lambda, x)}{\partial \lambda} \Big|_x \tag{5.9}$$

$$f_{field} = -\frac{\partial W_{field}(\lambda, x)}{\partial x} \Big|_\lambda \tag{5.10}$$

The partial derivatives are evaluated while holding x and λ, specifically x for Equation 5.9 and λ for Equation 5.10. This enables us to compute the mechanical force.

$$f_{field} = -\frac{\partial}{\partial x}\left(\frac{1}{2}\frac{\lambda^2}{L(x)}\right) \Big|_\lambda = \frac{\lambda^2}{2L(x)^2}\frac{dL(x)}{dx} \tag{5.11}$$

This equation simplifies to a derivative with respect to x:

$$f_{field} = \frac{i^2}{2}\frac{dL(x)}{dx} = \frac{i^2}{2}\frac{\mu_g N^2 l}{2g} \tag{5.12}$$

The variables g and l are the dimensional parameters air gap height and core thickness respectively, of the coil depicted above in Figure 2.5. Now we have a model to compute the force of the actuator as a function of the current and physical properties of the materials.

5.2 Design Process

5.2.1 Initial Conceptual Design

The design process of this reluctance actuator consisted of several design iteration to achieve an acceptable device. Figure 5.1 displays the first conceptual design of the actuator. It is designed to actuate in two directions, labeled x and y. One of the key advantages of this design is its simplicity. It consists of two mirrored designs: a C-shaped actuator on the left and right to control motion in the x-direction and a U-shaped actuator on the top and bottom to control motion in the y-direction.

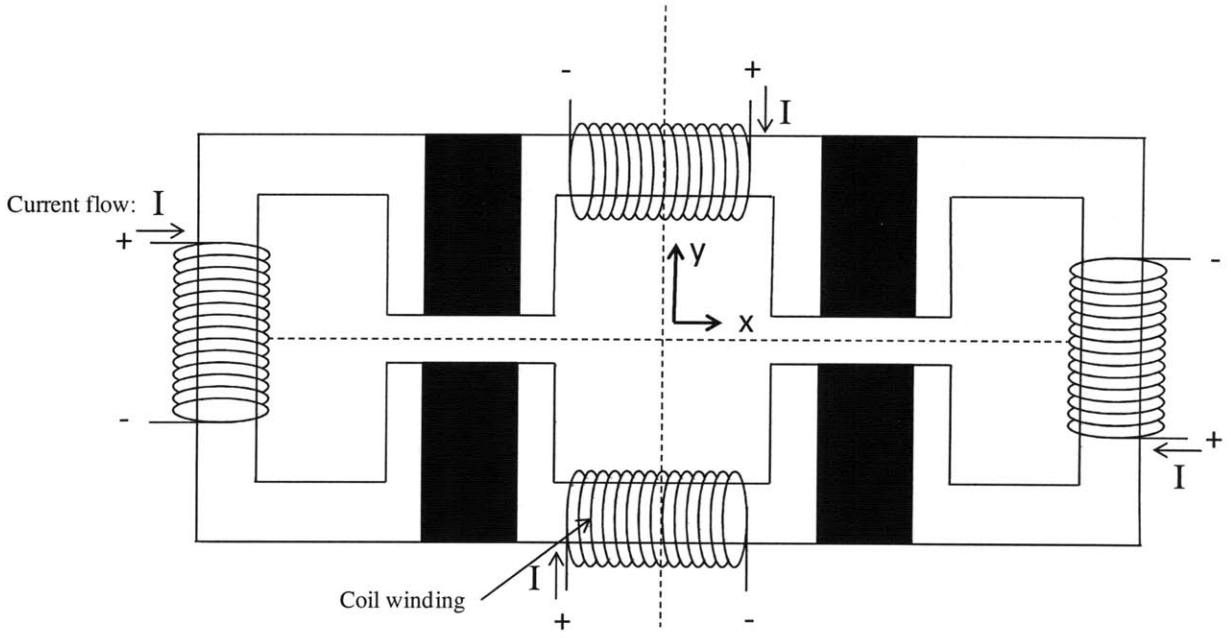

Figure 5.1: Initial actuator conceptual design

Figure 5.2 displays the path that the magnetic field lines follow as they flow through the magnetic cores completing their individual circuits. Magnetically insulating material was required to prevent the device from "magnetically short circuiting." This material should be thicker than the air gap. A simple rectangular-shaped plunger was initially proposed as the recipient of the forces imposed by the actuators. This plunger would be rigidly attached to the tabs of the Hexflex and transfer the forces from the actuator to the Hexflex.

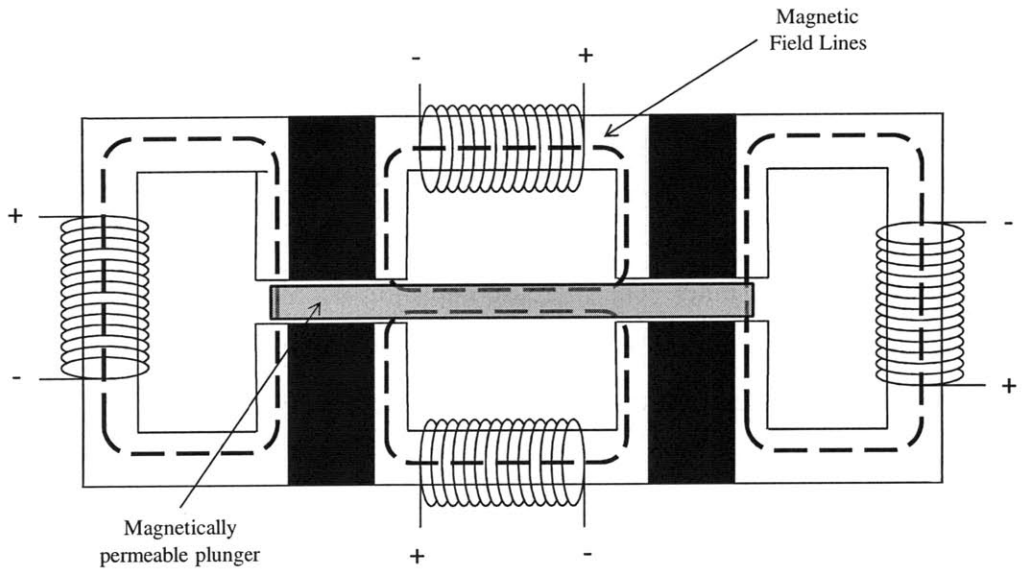

Figure 5.2: Actuator concept diagram displaying "ideal" flow of magnetic field lines

5.2.2 Revised Design

This initial design was revised and a second design was proposed. The new design is shown in Figure 5.3. This design expanded upon the symmetry of the first design and incorporates C-shaped actuators to replace the previously proposed U-shaped actuators. This simplifies the entire design enabling a single actuator design to be used for all four previous sides of the device. This also allows the forces for the actuators to be calculated using the same governing equation.

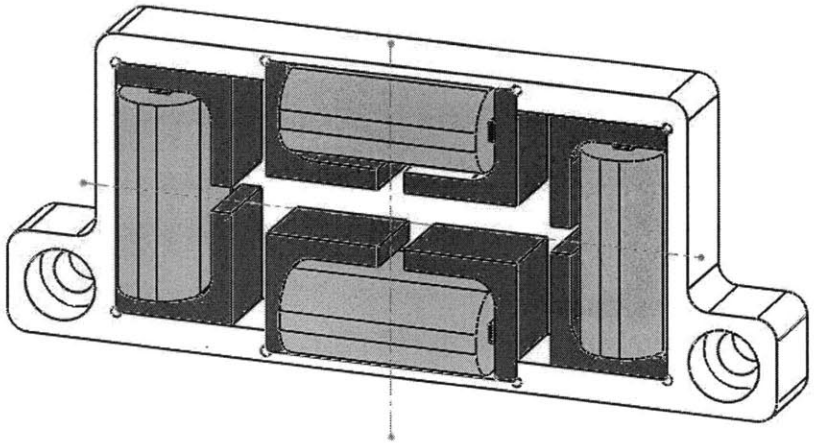

Figure 5.3: Solid model of reluctance actuator

This design incorporates a "shell" for the four actuators. This shell confines the actuators and also provides a structure that may be used to attach the device to a base or platform when it is integrated into a system with the Hexflex.. This shell also provides some degree of rigid support for the individual actuator sub-units, constraining them so as to prevent deformation of the C-shaped actuators under the magnetic forces. The shell also appropriately aligns and spaces the actuators in an orthogonal manner. The increased spacing decreases the likelihood of magnetic short circuit developing by positioning the individual actuators far enough away from each other such that the resistance created by their air gap prevents any unwanted interactions between the actuators.

As shown in Figure 5.4, this design divides the C-shaped actuator into three pieces. This is done to allow efficient and proper winding of the coil that will induce the magnetic field. The central rectangular piece acts as a mandrill and is wound with magnetic wire. This piece is then rigidly attached to the outer L-shaped pieces to form the complete C. The rectangular mandrill and L-shaped pieces are all also simple in geometry and remain consistent with the overall design goal of simplicity and manufacturability.

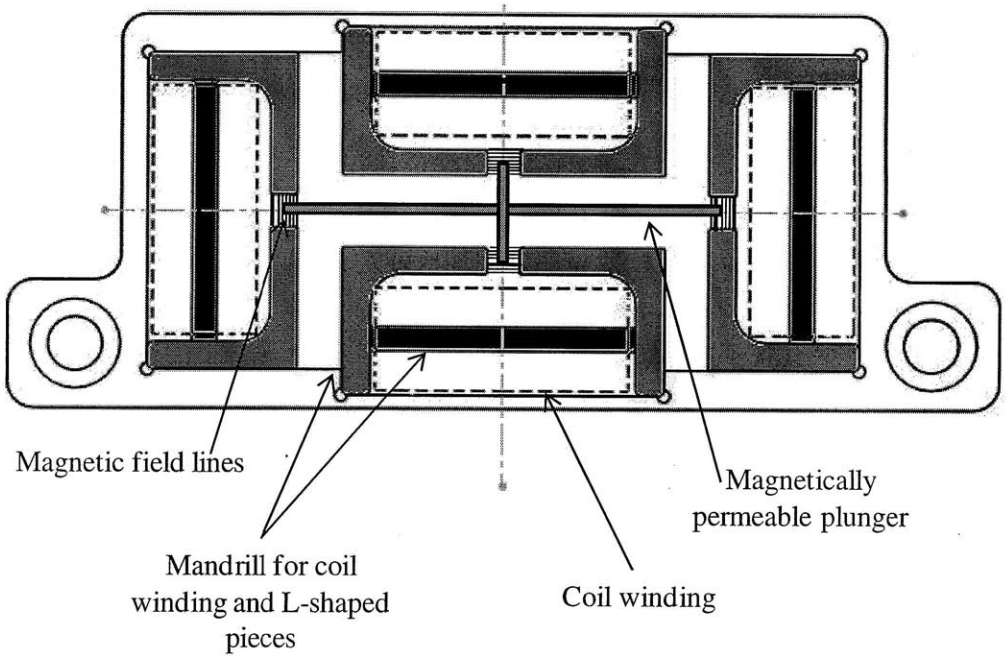

Figure 5.4: Top view of reluctance actuator displaying plunger and components

In this design a cross shaped plunger is proposed to enable appropriate x and y actuation. In this design the edges of the plunger must cross the magnetic field lines for forces to be generated on it. Furthermore, the two axis do not interfere with one another since the force generated is dependent on the depth, number of magnetic field lines crossed, and not the height at which the plunger crosses them. In other words, the number of field lines which the plunger crosses is the important factor as opposed to the position or height at which those lines are crossed. Figure 5.5 illustrates this concept.

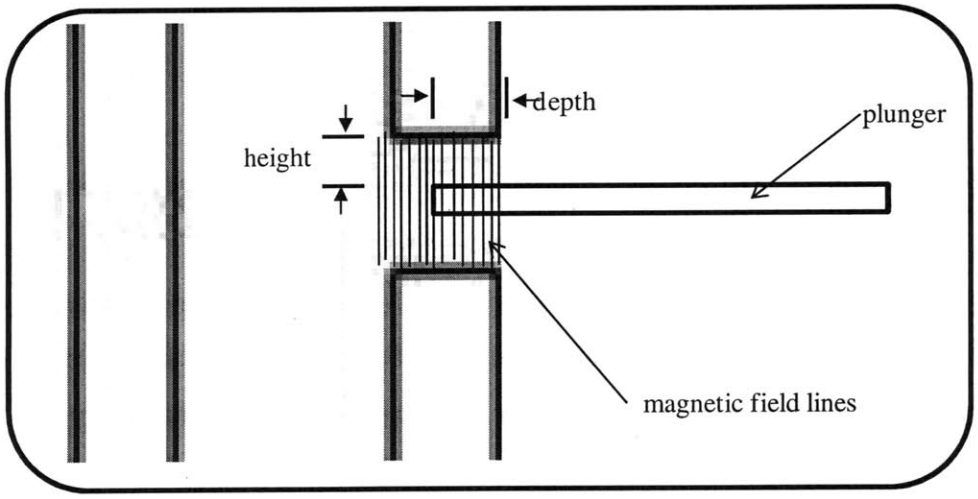

Figure 5.5: Close-up diagram displaying actuator functionality

It is noteworthy to mention that a new constraint is introduced with this design. The range of the actuator, e.g. how far the plunger may be displaced, is dependent on the air gap spacing of the C-shaped actuators. For example the displacement in the x direction is limited by the air gap spacing of the actuators which control the y axis. This limitation may be remedied by adjusting the thickness of parts of the plunger or adjusting the height of the air gap. If the height of the air gap is increased, then equal ranges in the x and y axes, will require the device to increase in size in both directions. The x and y dimension have become interconnected.

Careful attention must be paid to the space constraints of the actuation device due to (i) the aforementioned coupling of the x and y dimensions and (ii) the confinement of the shell. As the force is directly proportional to the number of turns in the coil and space constraints, the coil must be wound in a precise and particular manner. The coil requires a minimum number of turns

to work effectively but must also fit those turns within a certain cross-sectional area. This requirement influences the height of the mandrill and the distance at which the L-pieces extend away from it. This influence ultimately also affects the size and spacing of the individual actuators and the size of the actuator shell. In order to meet the 600 turn requirement, space requirement, and minimize the device size, the coil was wound with ten rows of sixty turns each using AWG 26 wire.

5.2.3 Backplate Revision

Although the revised design allowed for effective winding of the mandrill it decreased the strength of the actuator sub-unit as it was divided into three pieces and held together by epoxy. Due to the nature of the magnetic circuit, forces will act to pull the L-pieces together, to close the air gap which will in turn create stress concentrations within the epoxied joints of the magnetic core. These forces could break the epoxy bonds at the joints of the L-pieces and the mandrill. A "backplate" was developed to remedy this weakness. This plate was a sheet of aluminum approximately 1/8" in thickness that had a similar outline to the actuator shell. The side faces of the actuators would be epoxied to the backplate as shown in Figure 5.6. Epoxy can withstand greater shear stress than tensile stress and consequently the epoxy bonds holding the side actuator against the back plate withstood the stresses generated by the magnetic field lines.

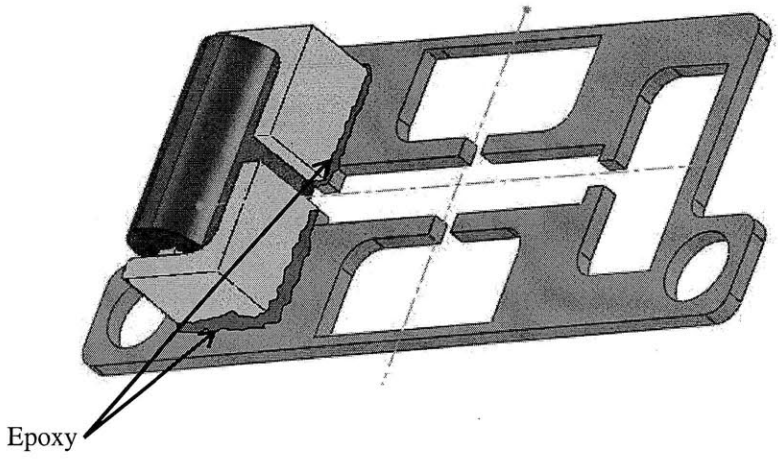

Figure 5.6: Solid model illustrating actuator assembly process

5.3 Prototype Manufacturing

As the actuator is mostly composed of simple two dimensional structures, water jetting is one of the most ideal means of manufacturing its parts. This method allows for quick and relatively low-cost manufacturing while also providing accurate parts. Parts may easily be created from DXF files. The L-pieces of the core, mandrill, backplate, plunger, and actuator shell were all cut from aluminum and magnetic steel. This method is most ideal when using thin material; unfortunately, as the material increases in thickness, beyond approximately 1.27cm (0.5in), precision, time, and cost significantly increase.

5.3.1 Assembly Process:

Coil- The coils for the actuator for this prototype were hand wound by placing the mandrill into a lathe and spinning the spindle while simultaneously guiding the magnetic wire as it wrapped around the mandrill. A coating of super glue was applied to each layer of windings to secure the coils and to prevent them from unwinding as soon as the wire was released. For small quantities of coils, this is the most cost effective way of producing the coils although it is labor intensive.

Actuator sub-unit assembly- The actuator sub-unit, the L-pieces, and the wound coil, is held together with epoxy. This assembly requires particular fixturing in order to ensure that the mandrill is attached at an appropriate distance from the front of the L-pieces and to also ensure that the three pieces are relatively square to one another. This accomplished by resting the L-pieces on a flat surface in their appropriate arrangement and placing two U-shaped pieces of aluminum alongside of them to "fence" in the pieces and ensure that they are co-linear. Superglue is applied to the ends of the mandrill and to the L-piece. A rectangular block is placed behind either L-piece and used to compress the two L-pieces towards each other after the mandrill has been lowered into position between them. The superglue forms a quick but weak bond between the pieces. If the alignment is satisfactory, epoxy is then applied to the joints and the sub-unit is allowed to cure. Figure 5.7 shows this process.

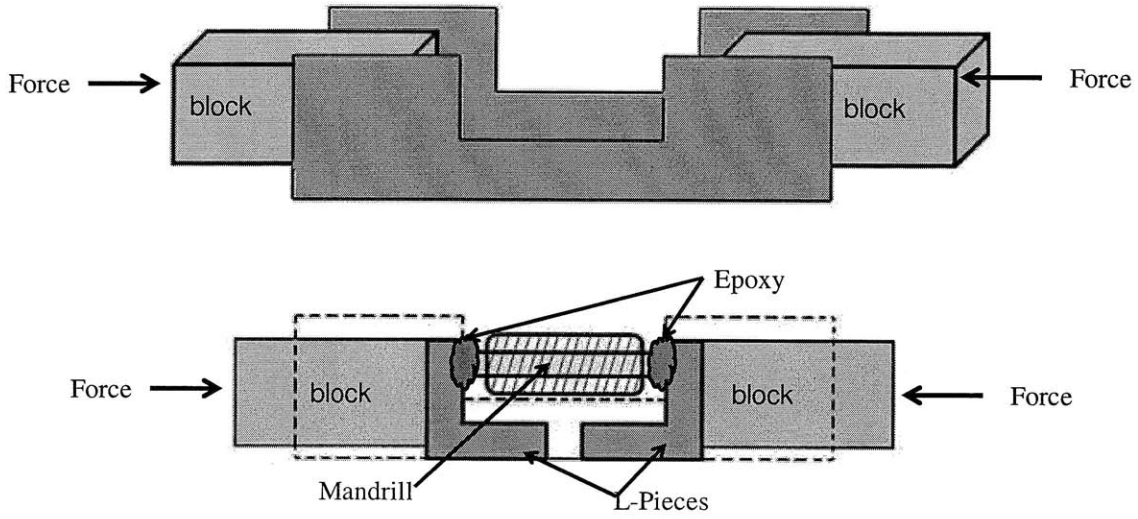

Figure 5.7: Diagram illustrating assembly process for actuator sub-units

Complete actuator device assembly- After the assembly, the actuator sub-units are individually placed into the actuator shell. They should slide snuggly into place with the sides of L-pieces aligning flush with the side of the actuator shell. Finally the backplate should be epoxied onto one side of the actuator shell, bonding to the shell and all four of the individual actuator sub-units.

Plunger Assembly- The plunger is epoxied onto the end of the Hexflex tabs.

5.3.2 Manufacturing Changes:

After constructing the first actuator sub-unit, cost and time saving changes were implemented. The dimensions of the L-pieces are similar to those of standard angle-iron. This iron can be easily modified via light machining, milling the ends, to achieve desired lengths and subsequent chopping via a saw to the appropriate thickness. Furthermore, the plunger design was revised to be cut in two pieces out of a sheet of magnetic steel and assembled perpendicularly as opposed to the initial monolithic one piece design shown in Figure 5.8.

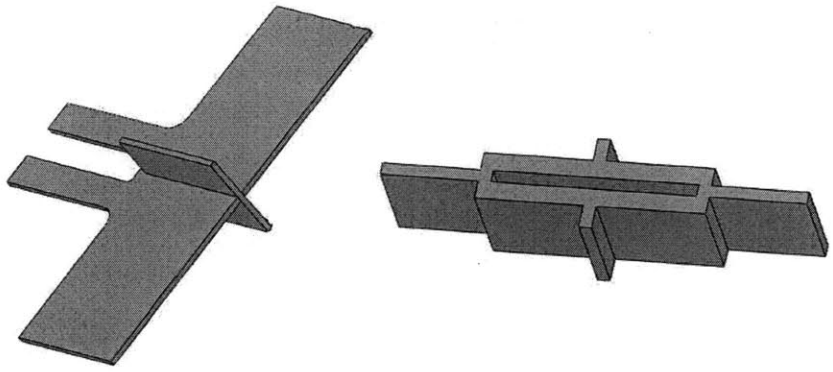

Figure 5.8: Initial plunger design (right) and revised design (left)

5.3.3 Assembly Problems and Modifications:

After constructing a complete actuator, several observations were made to improve the quality and efficiency of the assembly process. The manner in which the parts were being assembled resulted in inconsistencies amongst the heights of the air gap for the various actuator sub-units.

Furthermore, the central axis of symmetry for a particular individual actuator sub-unit was not collinear with that of its opposing actuator sub-unit. These inconsistencies resulted from attempts to simultaneously constraint multiple degrees of freedom while assembling and gluing the actuator sub-units. Moreover, the liberal use of epoxy as the primary bonding agent for the joints and interfaces decreased the accuracy of the actuator subunit assembly.

The misalignments resulting from the above mentioned issues and also poor manufactured part quality resulted in a significant decrease in the effectiveness of the backplate. The plate was not able to effective align flush with the sides of the actuator sub-units and consequently could not effectively adhere to their surfaces. The actuator shell proved to be rigid enough to prevent significant deformation from the internal magnetic forces of the actuators.

Another revised design was developed to remedy these issues. This design eliminates the actuator shell and relies on the backplate as the primary means of part alignment. Figure 5.9 illustrates the design, wherein small screws are used as a means of positioning the actuator sub-units. These screws are also ideally positioned so as to oppose the internal forces generated by

the actuators and to reduce the stress within the sub-unit. Furthermore the backplate and screws aid in correcting the alignment problems by affixing the subunits to a common surface. The screw holes may be precisely cut into the backplate in their "ideal" positions and misalignment errors can be resolved by over-sizing these screw holes and using a nut to secure the parts in the appropriate position.

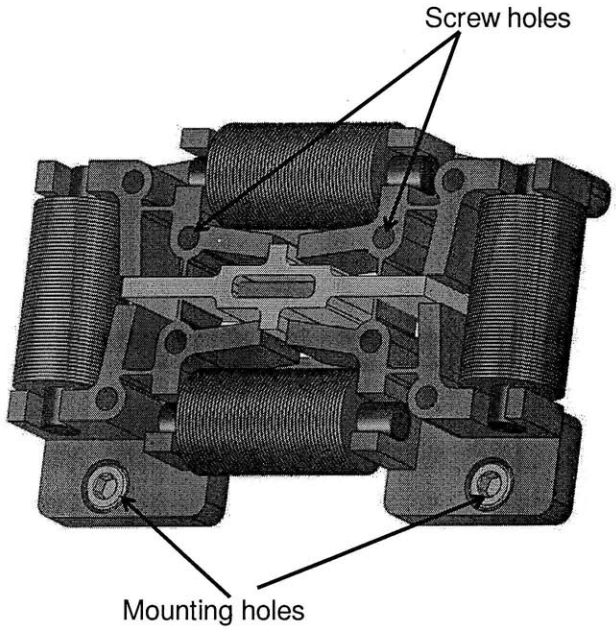

Figure 5.9: Solid model of post-manufacturing revised design (Thanks to Martin Culpepper and Robert Panas for this design)

The sub-unit still consists of three pieces; however, the mandrill is constructed from cylindrical steel rods as opposed to rectangular steel blocks. This change allows for easier winding and the rods may also be press fit into holes bored into the L-pieces, eliminating the weakness created by primarily relying on the epoxy joints for structural stability.

CHAPTER

6

VALIDATION

6.1 Design and Manufacturing of Test Apparatus

A testing apparatus was design and built to calibrate the actuator and to aid in the design and development of a complementary control system. This test apparatus consisted primarily of a planar flexure and capacitance probes. This apparatus would be attached to the actuator with the plunger super glued to the center of the flexure. Figure 6.1 shows the apparatus set-up. The capacitance probes contact the rectangular block which is centered and adhered to one side of the central "stage" of the flexure. This apparatus was designed to measure the displacement in this central stage, via the block, while the actuator was activated. This displacement could then be used with the stiffness of the flexure to determine the amount of force that the actuator was outputting which could then be compared with our predictions.

6.1.1 Flexure

The flexure shown in Figure 6.1 permits movement in x and y. The flexure is designed to be stiff enough to move in either direction by approximately 120 microns with 5N of force. This design ensures that the displacement of the flexure remains within the range of the capacitance probes. The flexure design was also merged with the template for the actuator shell to enable easy attachment to the actuator.

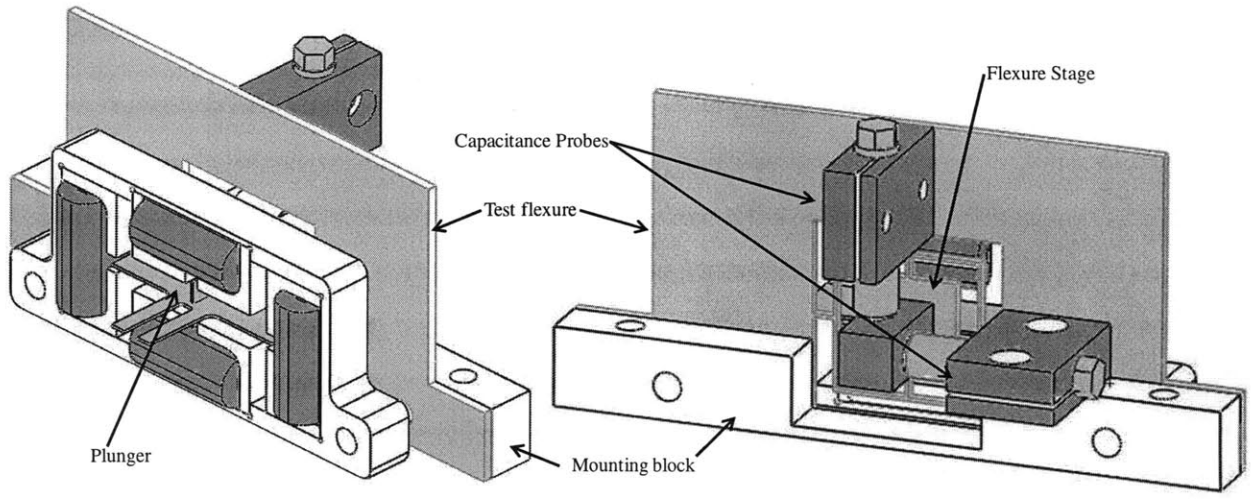

Figure 6.1: Solid model of testing actuator and testing apparatus

Finite Element Analysis was performed to ensure that the design requirement was met and to verify that the flexure will not fail under the desired parameters. Screenshots of this analysis are shown in Appendix A.

6.1.2 Manufacturing

The flexure was manufacturing via water jet from 2.54mm (0.10 in) thick aluminum.

6.2 Force Testing

An actuator was connected to a power supply which circulated currents ranging from 100 to 700mA. A piece of magnetically permeable steel was position in the air gap in one of the actuator sub-units. It was observed that the steel had a tendency to attract to either the top or bottom face of the air gap. At approximately 700mA, less than half of the actuators maximum current, tactile feedback alone suggested that a considerable amount of force was applied to the piece of metal holding it against the sub-unit. The steel piece was again positioned in the gap and after a short period of probing with the steel and observing the response, it was noted that no significant force was actually pulling the steel into the air gap. Forces were acting; however, the subunit seemed to be functioning as a magnet. The steel would attract to the side of the air gap and front of the individual sub-units as illustrated in Figure 6.2.

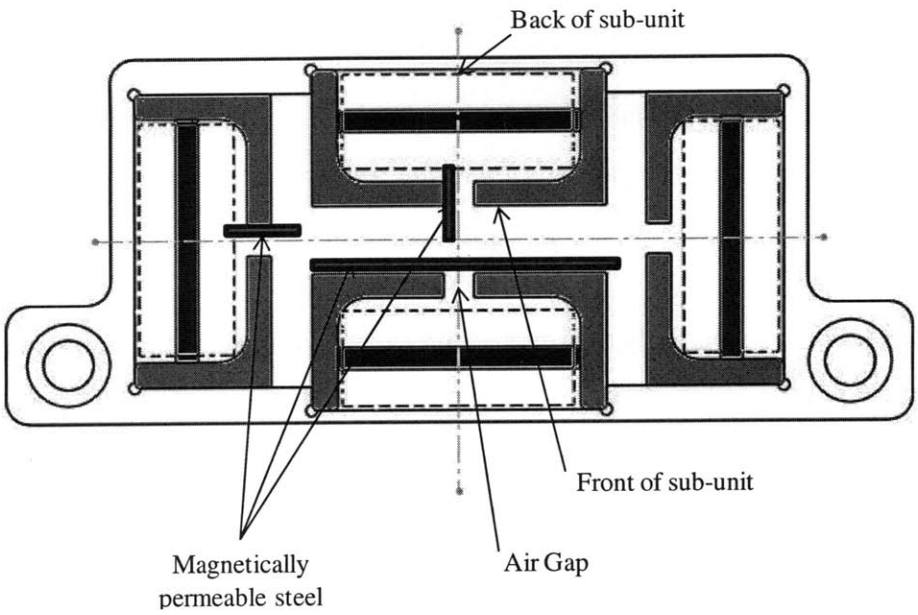

Figure 6.2: Magnetically permeable steel behavior in response to active actuator

These observations led to a re-evaluation of the actuator magnetic circuit modeling and assumptions. It was noted that certain assumptions made in the governing equations had not in fact been fulfilled during the production of the actuator.

The magnetic fields utilized by the reluctance actuator are normally highly non-linear; however, by making several assumptions it is possible to simplify the governing equations and produce an actuator which operates in the linear regime of these magnetic circuits. One assumption that is necessary for the actuator to function properly is that the plunger thickness h must be much greater than the air gap g as shown in Figure 2.5. This means that the plunger must be at least two orders of magnitude larger than the air-gap, g, which will surround it. What actually was happening in the tested actuator was that the air gap was sufficiently small for the magnetic field lines to jump across without the aid of a plunger. In order for the reluctance actuator to work properly, the gap needs to be large enough such that the magnetic field lines require the presence of a magnetically permeable material to complete the circuit. Thus the actuator that was tested was merely functioning as a magnet.

Furthermore, the positioning of the actuator sub-units with respect to one another was too compact. Although this positioning was essential to minimize the size and bulk of the entire actuator, the air gap between the sub-units was sufficiently small to allow the individual sub-units to short circuit and jump the gaps from one sub-unit to another. This further reduced the correlation between our model and the actual manufactured actuator.

The $h>>g$ assumption was partially overlooked in efforts to minimize the size and material costs of the actuator. This resulted in unacceptable performance. Unfortunately, efforts to remedy this make this type of actuator unfeasible for such small scale application unless 1) sufficient space is available, 2) sufficient mechanisms are in place to effectively and precisely transfer forces from the large plunger to the smaller Hexflex, and 3) sufficient funds and material is available to manufacture the larger actuators.

CHAPTER 7

CONCLUSION

7.1 Summary of Actuator Development

A two-axis reluctance based actuator was designed to be used as part of a kinematic coupling assembly station utilizing the Hexflex compliant mechanism to achieve nano-scale precision positioning. This actuator explored a new technology employing the tangential reluctance force generated by a magnetic coil The performance characteristics of the reluctance actuator were compared to those of other actuators to verify it feasibility for this particular application. The development and investigation of this class of actuators, its design requirements, and manufacturing techniques, will provide future researchers and scientists with an increased capability to develop and produce actuators that are suitable for use in nano-scale manufacturing.

Various design requirements were identified and used to frame and focus the development of the actuator. A magnetic circuit governing model was developed to aid in the design this device and several design iterations were completed to develop an optimized actuator. After the design was completed the actuator was manufactured, and this production process was revised and improved to yield higher quality and more cost effective actuators. These revisions and other observations made during the manufacturing process in-turn had an effect on the design of the actuator ultimately leading to a concept that was optimized for assembly, cost effectiveness, and quality. After the production of the actuators, testing was conducted to evaluate the devices performance and to compare this to the predicted values. Observations led to the theory that various necessary assumptions which were vital to the proper functioning of the actuators were not adequately upheld in the manufactured product. This resulted in the actuators acting as electromagnets and not producing the desired performance.

The cause of this poor performance was explored resulting in the conclusion that it is not feasible to produce a two-axis reluctance based actuator of an appropriate size suitable for this application. It is theoretically possible to create a two-axis reluctance actuator if strict adherence to governing assumptions is observed. Furthermore, the design and manufacturing considerations presented in this thesis should significantly aid in further development of this device.

REFERENCES

[1] Martin L. Culpepper, Gordon Anderson, "Design of a low-cost nano-manipulator which utilizes a monolithic, spatial compliant mechanism," *Precision Engineering- Journal of the International Societies for Precision Engineering and Nanotechnology*, vol. 28, pp. 469-482, 2004.

[2] Anderson, Gordon. A six degree of freedom flexural positioning stage Master's Thesis, Massachusetts Institute of Technology, Cambridge, 2003.

[3] A. E. Fitzgerald, Charles Kingsley Jr., and Stephen D. Umans, "Electric Machinery," 6th ed., New York, NY: McGraw-Hill, 2003.

[4] David Jiles, "Introduction to Magnetism and Magnetic Materials," 2nd ed., Boca Raton, FL: Chapman & Hall CRC, Taylor & Francis Group, 1998.

[5] A. P. Dorey and J. H. Moore, "Advances in Actuators", London, UK: Institute of Physics Publishing, 1995.

[6] Cedrat Technologies, "Magnetic actuators & motors technologies," accessed April. 2010, <http://www.cedrat.com/en/technologies/actuators/magnetic-actuators-motors.html>.

APPENDIX A
ANALYSIS

A.1 Finite Element Analysis of Test Flexure

A desired displacement of 120-150μm was used as the boundary condition for this analysis. The two holes were fixed while a force of 5N was applied to the right face of the small square stage. The deformation of the flexure and the stress generated within the flexure are shown in Figure A.1, Figure A.2. Note that the flexure does not reach its yield stress.

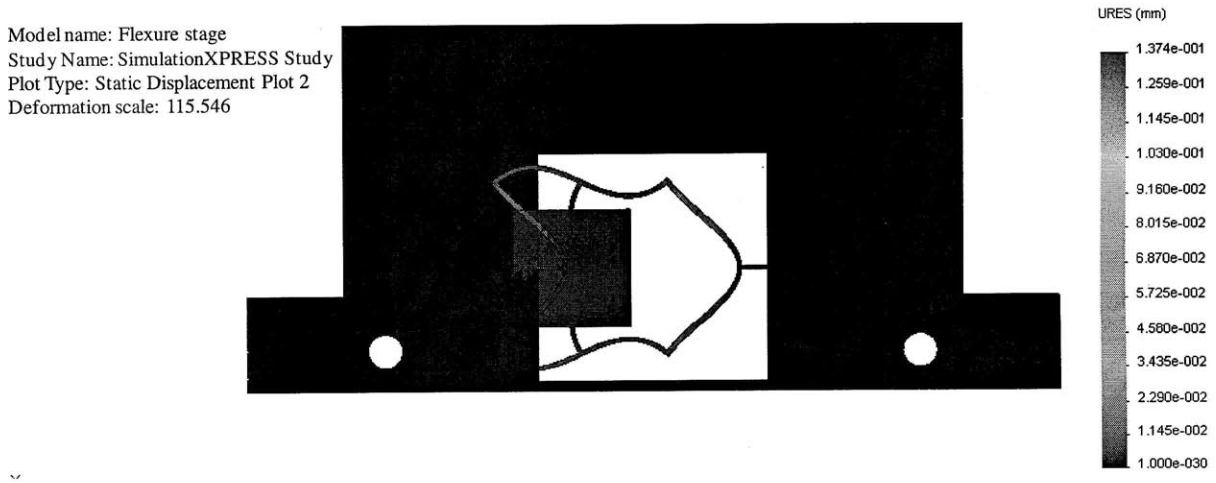

Figure A.1: FEA displacement model of test flexure

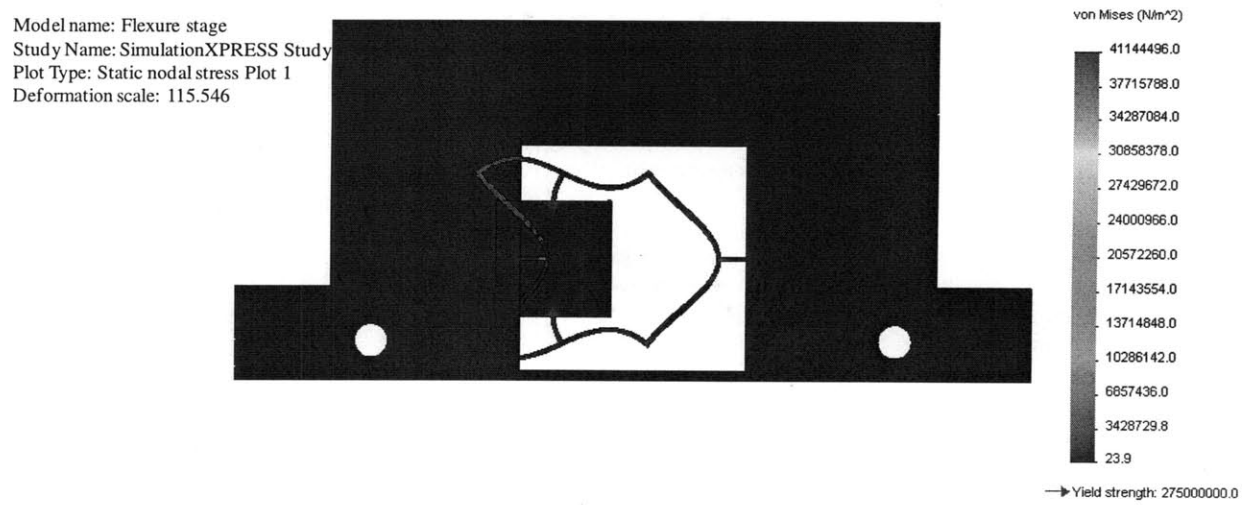

Figure A.2: FEA stress model of test flexure.

A.2 Magnetic Circuit Model

An Excel spreadsheet was used to compute the governing equations. This spreadsheet calculates the theoretical flux, forces, and displacement of the actuator given the necessary input values.

Howard Liles
Magnetic Circuit
Reluctance Actuator Design Project

Values	Units	Variable	Definition
1.26E-06	N / A^2	u_0	Permeability of free space
8.75E-04	N / A^2	u_c	permeability of magnetic core (magnetic steel)
1.26E-06	N / A^2	u_g	permeability of air gap
0.00125	m	g	height of air gap (one side of plunger)
0.003	m	q	width of C (when viewed from above)
0.0127	m	p	depth of C (when viewed from above)
0.0015	m	x	distance into C
600	#	N	number of coil turns
2.2	A	i	Current
0.022352	m	a	X Length of C
0.024892	m	b	Y Length of C
0.004572	m	m	C leg thickness
0.001526	m	p_height	Plunger height
0.004026	m		C spacing

Descriptions:	Value	Units
Length of central X axis	0.019352	m
length of central y axis	0.02032	m
Mean core length	0.079344	m
Air gap Cross sectional area	0.00001905	m^2
C-Cross sectional area	0.0000381	m^2
Inductance	0.003447207	H
Reluctance of Core	2380022.497	A*turns/Weber
Reluctance of air gap	52216188.74	A*turns/Weber
*Total Reluctance	54596211.24	A*turns/Weber
*in series		
Magnetic Flux	2.41775E-05	weber
Magnetic Flux density	0.634580102	Tesela
Stroke Length	0.0015	m
Force	-5.56149361	N
Number of turns	568.9060225	#

Refinement:
**For range of 2.5 mm, need q and g to be 5mm or greater
** ways to increase force: increase thickness of C, increase current, increase number of turns
**Thickness of C limit: basically no limit...
**current limit: thickness of wire
**number of turns limit: space available (thickness of wire)

Figure A.3: Magnetic modeling spreadsheet

APPENDIX B

EXPENDITURES

A spreadsheet was also used to record the expenditures of this research project.

Table B.1: Actuator material costs

Item	Price	Quantity	Total Price	Description:	Status	Purchase method
1.5 Hour Epoxy	$3.71	1	$3.71	Epoxy for Mandrill Coil Winding	Purchased	Reimbursement
Crazy Glue	$5.09	1	$5.09	Glue for Mandrill Coil Winding	Purchased	Reimbursement
Angle Iron	$11.16	1	$11.16	Low-Carbon Steel 90 Degree Angle 1/8" Thick, 3/4" Leg Length, 6' Length	Purchased	Richard: McMaster
Tinned Copper Wire	$20.47	2	$40.94	Tinned Copper Wire .020" Diameter, 1-lb Spool, 793' Spool	One item returned: wrong wire	Richard: McMaster
Low Carbon Sheet Steel	$41.66	1	$41.66	Low-Carbon Steel Sheet, 1/2" Thick, 8" X 8"	Purchased	Richard: McMaster
Stainless Steel	$66.93	1	$66.93	Stainless Steel, 1/2" Thick, 6"X6",	Purchased: Wrong type of steel	Richard: McMaster
Magnetic Wire	N/A	N/A	N/A	AWG 26	Borrowed from Edgerton	N/A (no payment necessary)

Table B.2: Water jet machining costs

Item	Price (per minute)	Quantity	Total Price	Time (minutes)	Status	Purchase method
Actuator Back**	$3	1	5.9634	1.9878	Completed	Requisition with Hobby Shop
Actuator Shell**	$3	1	38.853	12.951	Completed	Requisition with Hobby Shop
Mandrill**	$3	4	56.67	4.7225	Completed	Requisition with Hobby Shop
L-Pieces**	$3	4	81.84	6.82	Completed	Requisition with Hobby Shop
Plunger**	$3	1	52.992	17.664	Completed	Requisition with Hobby Shop
Actuator Back	$3	3	17.8902	1.9878	Completed	Requisition with Hobby Shop
Actuator Shell	$3	2	77.706	12.951	Completed	Requisition with Hobby Shop
Actuator Shell (Low Cut Quality)	$3	1	30	10	Completed	Requisition with Hobby Shop
Mandrill	$3	12	170.01	4.7225	Completed	Requisition with Hobby Shop
Plunger	$3	2	105.984	17.664	Completed	Requisition with Hobby Shop

** Indicates Pieces Made with Wrong Materials

Table B.3: Total costs

Total Water jetting Time (minutes):	212.6362
Total Cost of Water jet cutting:	$637.9086
Total Cost of Water Jet Cutting Using Wrong Materials:	$236.3184
Total Cost of Water Jet Cutting in Ideal Scenario:	$401.5902
Total Cost of Raw Materials:	$169.49
Total Expenditures for Research Project:	$807.3986

APPENDIX C

IMAGES AND DRAWINGS

The design specifications used to manufacture the actuator prototype are displayed in Table C.1. Furthermore, solid drawings display the dimensions, material and layout of the components that make up the actuator. Finally photographs of the test apparatus and actuator show the construct test setup and actuator prototype.

Table C.1: Actuator design specifications

Coil:	
Wire Type:	Magnetic Wire
AWG Size:	26 (0.403mm)
Number of Layers	10
Number of Turns Per Layer	60
Maximum Current Allowed	2.2 Amps
Wire Resistance	133.856 Ohms/Km
Core Pieces (L-Pieces and Mandrill):	
Material:	Low Carbon Magnetic Steel
Thickness:	1.27 cm
Width:	0.3 cm
Plunger:	
Material:	Low Carbon Magnetic Steel
Thickness:	0.076 cm
Actuator Shell:	
Material:	Aluminum (T6- 6061)
Width:	12.11 cm
Thickness:	1.27 cm
Length:	4.88 cm
Actuator Backplate:	
Material:	Aluminum (T6- 6061)
Width:	12.11 cm
Thickness:	0.3175 cm
Length:	4.88 cm

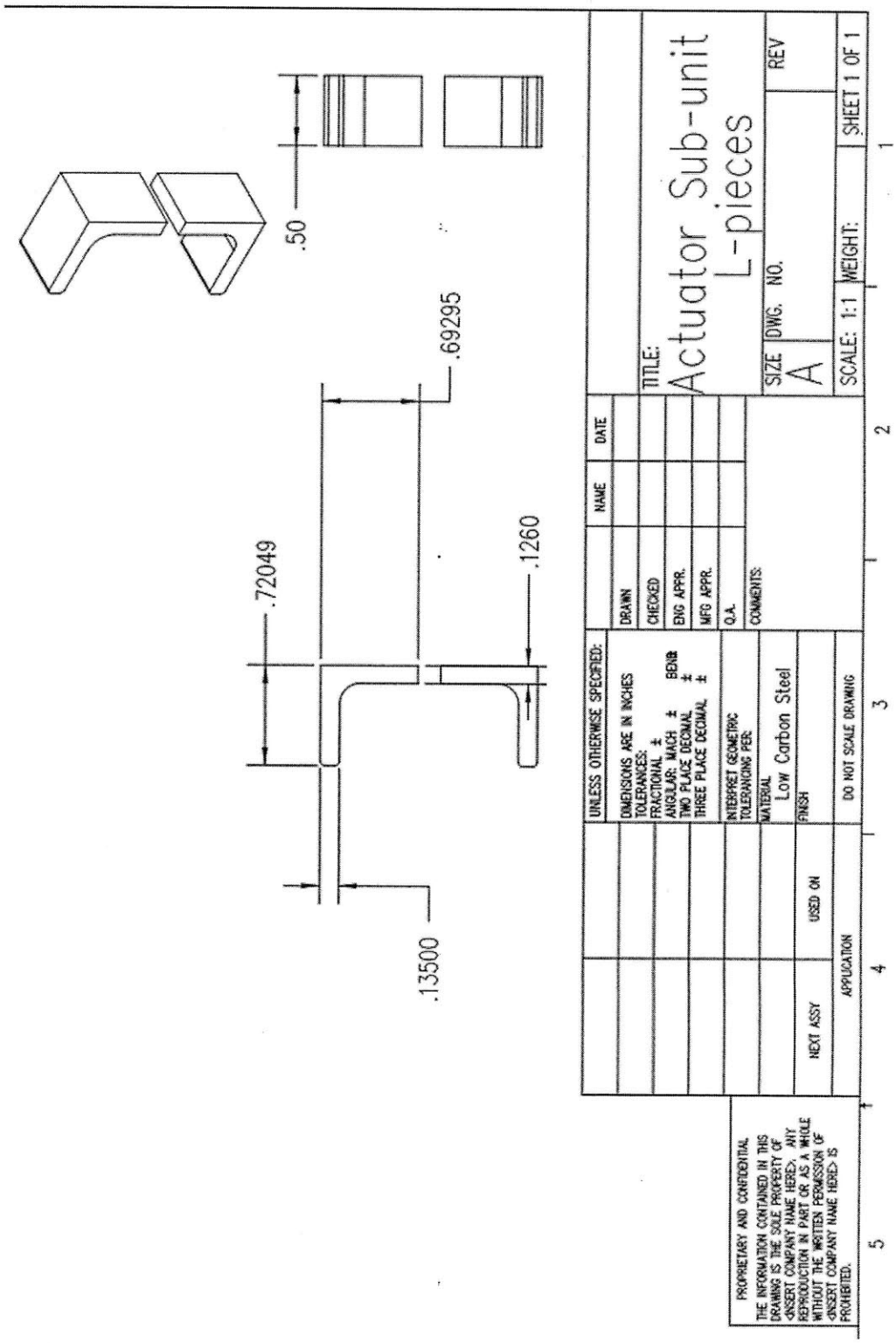

Figure C.4: Dimensioned drawing of sub-unit L-shaped pieces

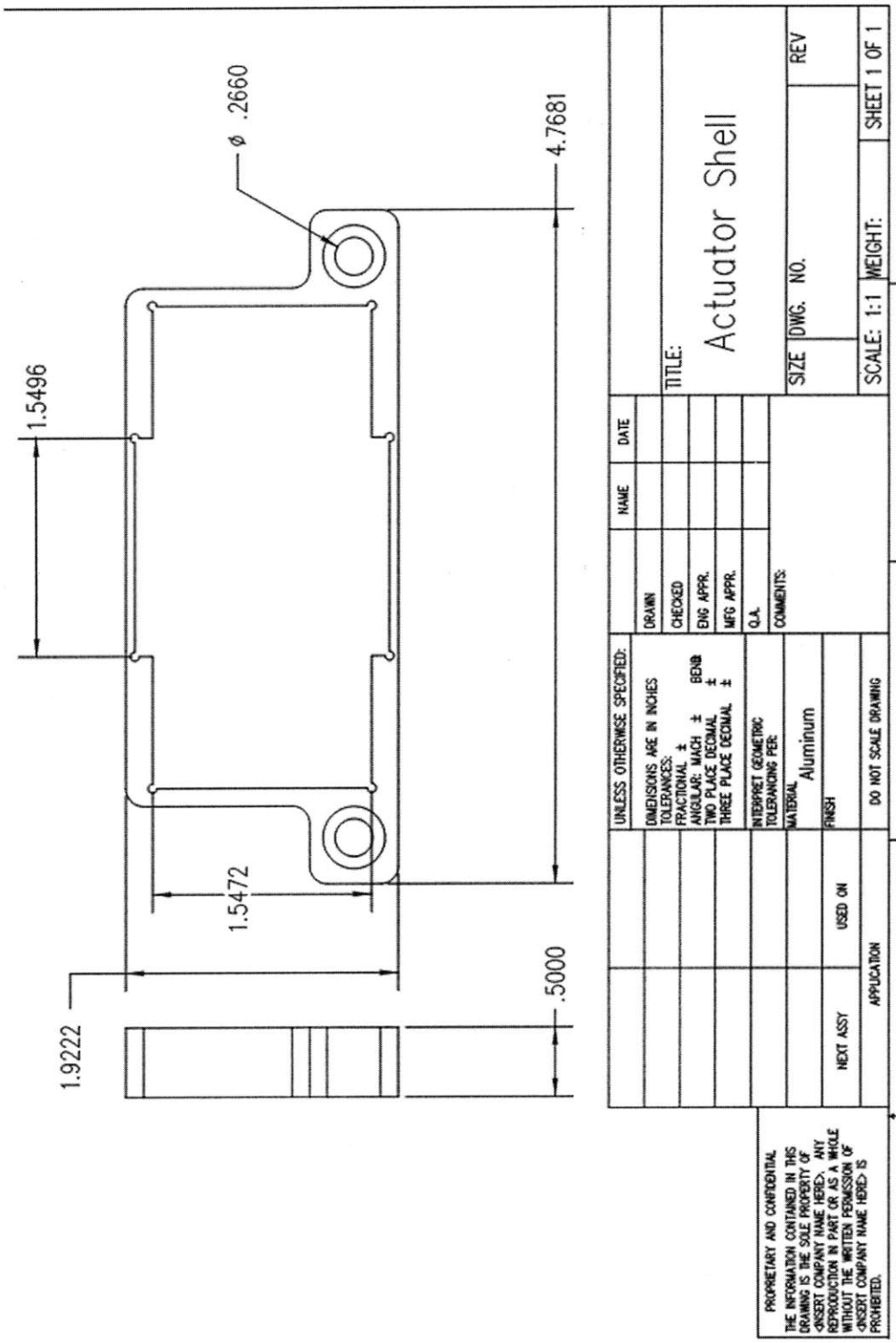

Figure C.5: Dimensioned drawing of actuator shell

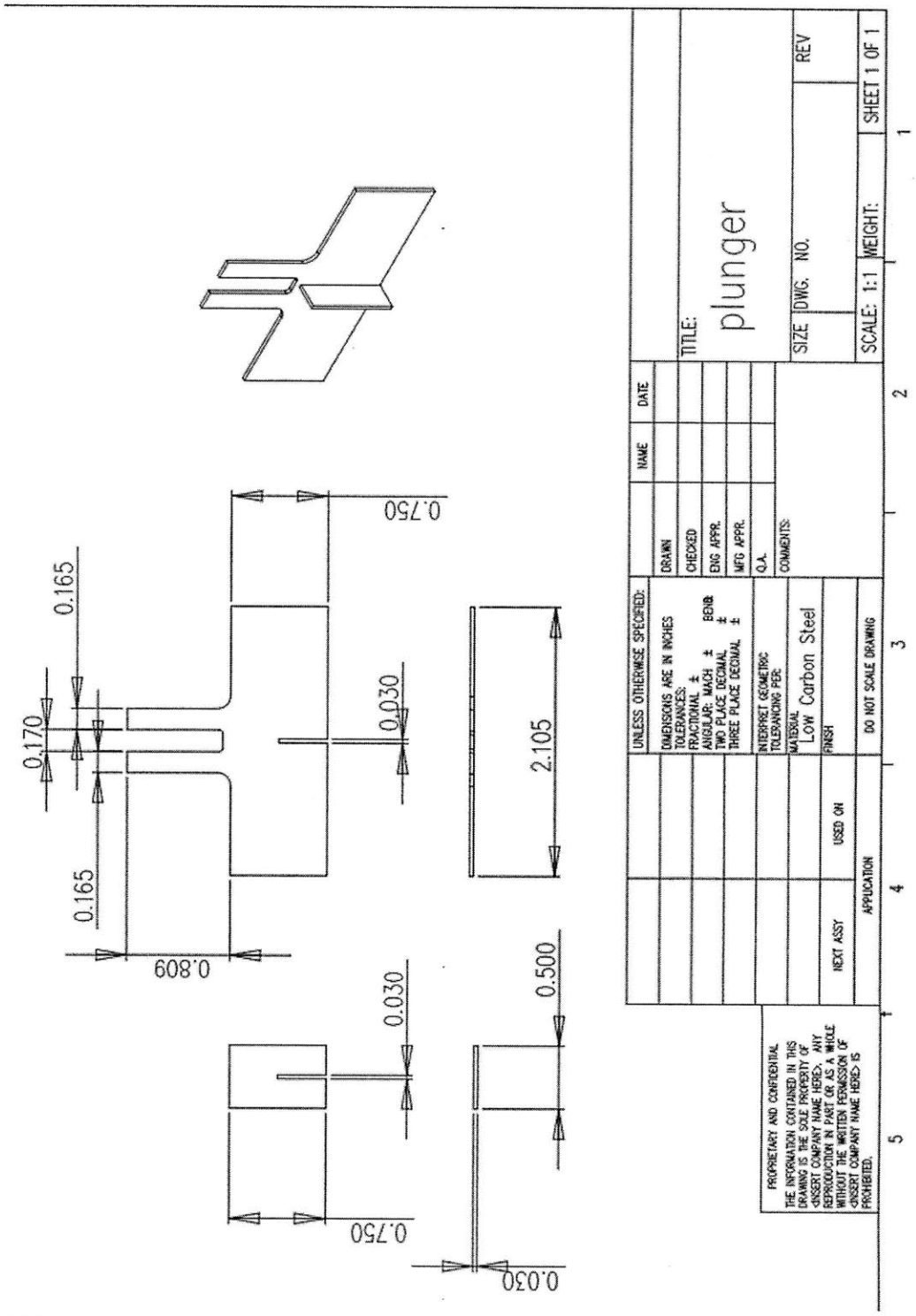

Figure C.6: Dimensioned drawing of revised plunger components and assembly

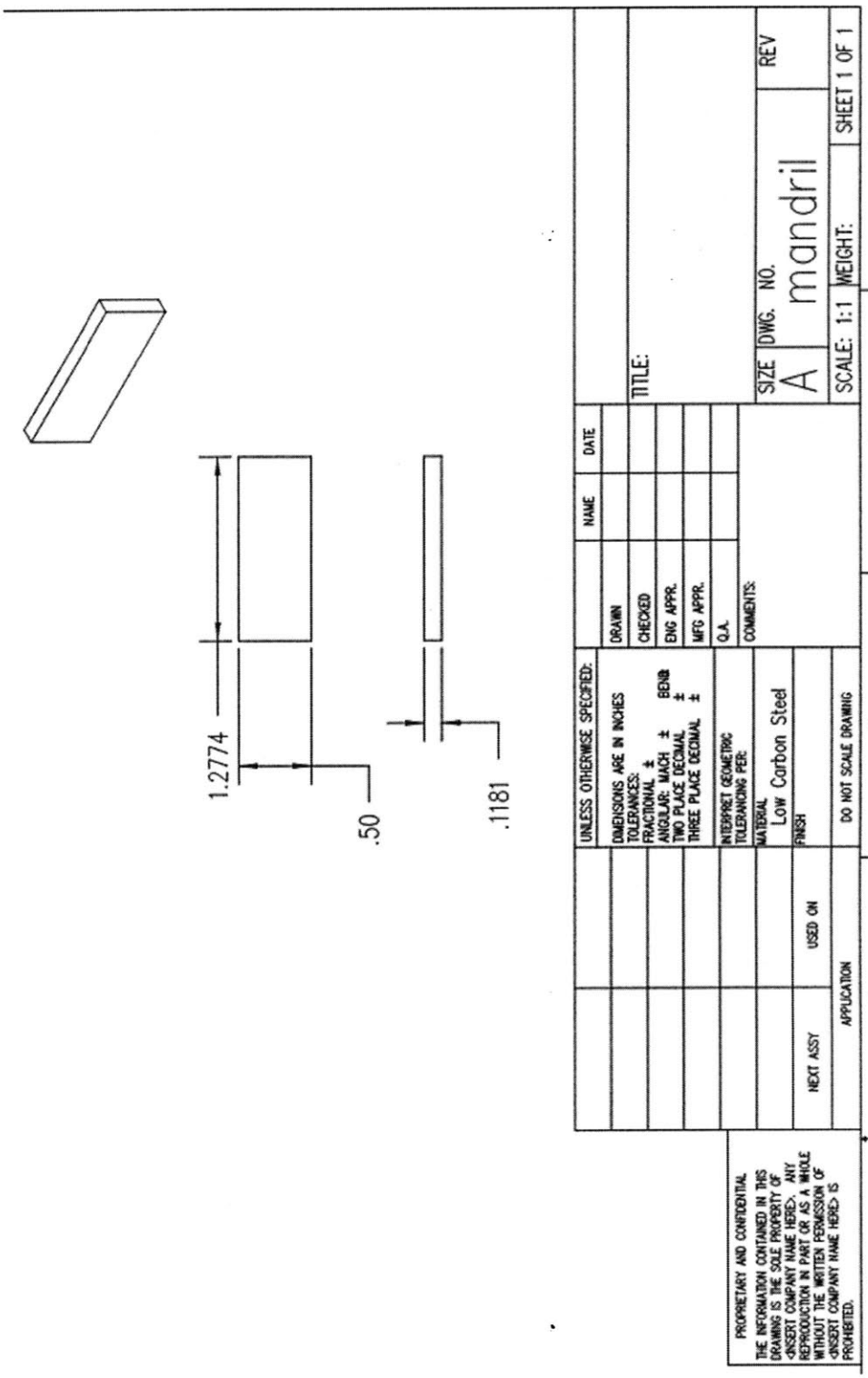

Figure C.7: Dimensioned drawing of rectangular mandrill used in actuator sub-unit

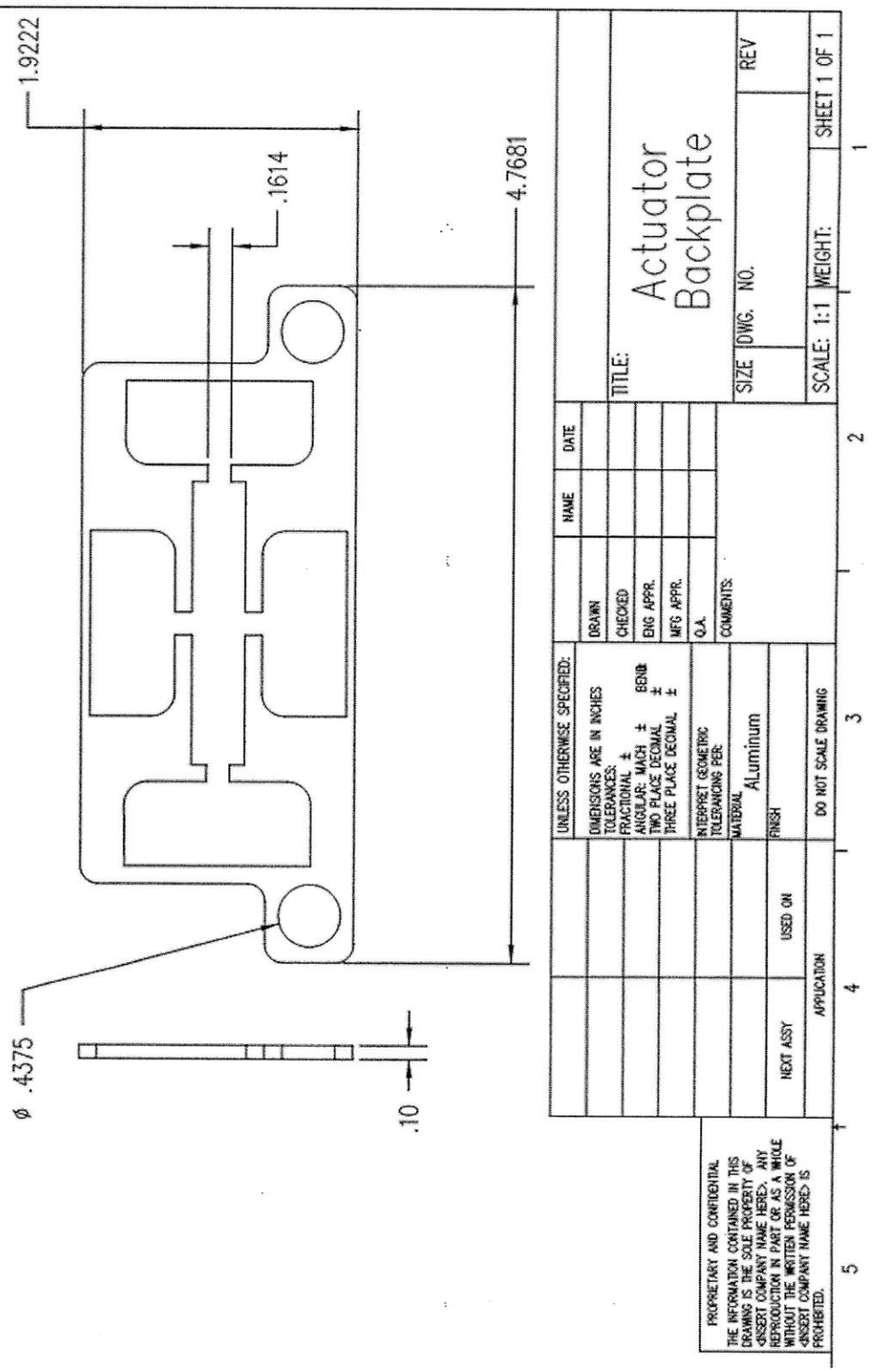

Figure C.8: Dimensioned drawing of actuator backplate

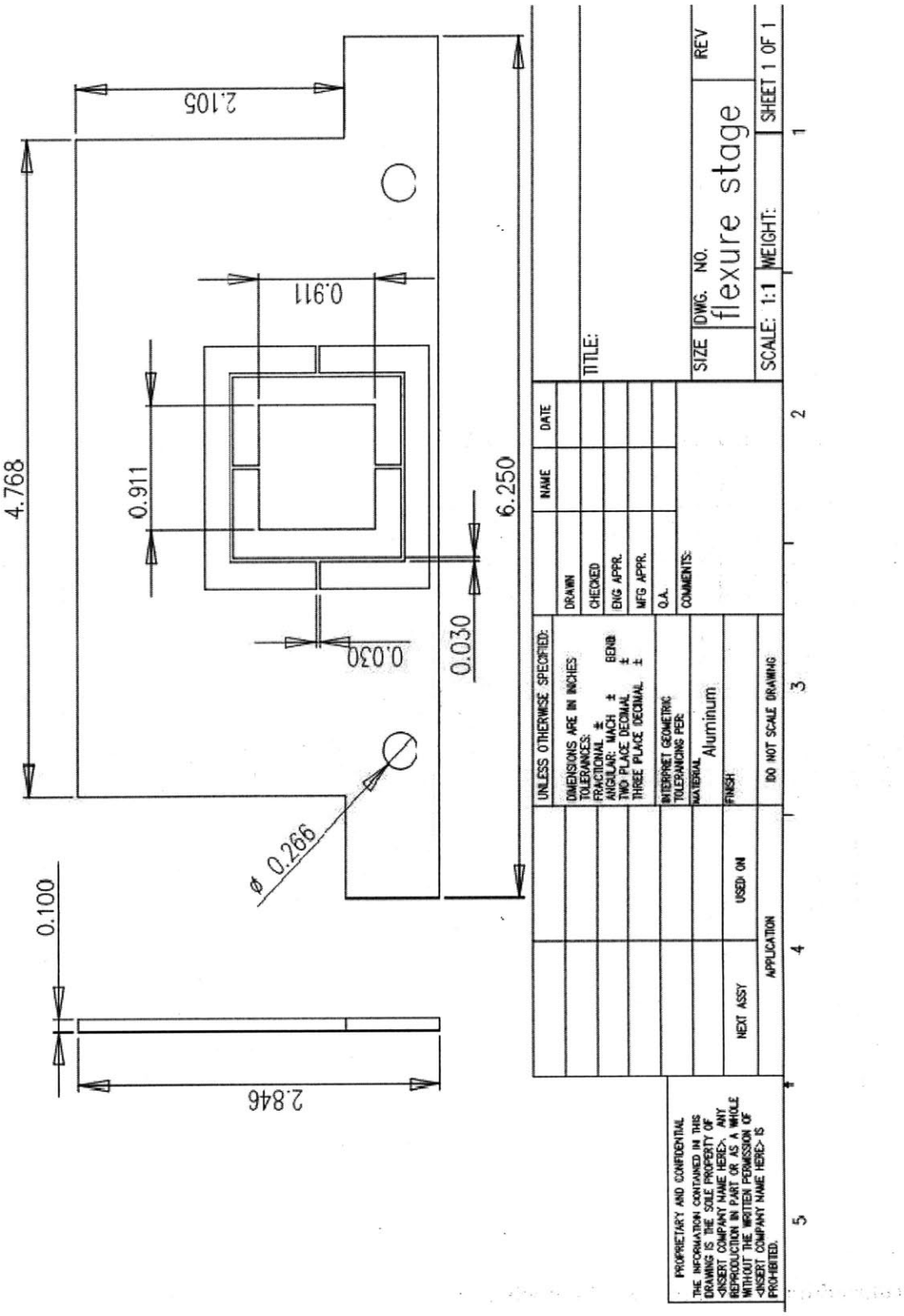

Figure C.9: Dimensioned drawing of test flexure

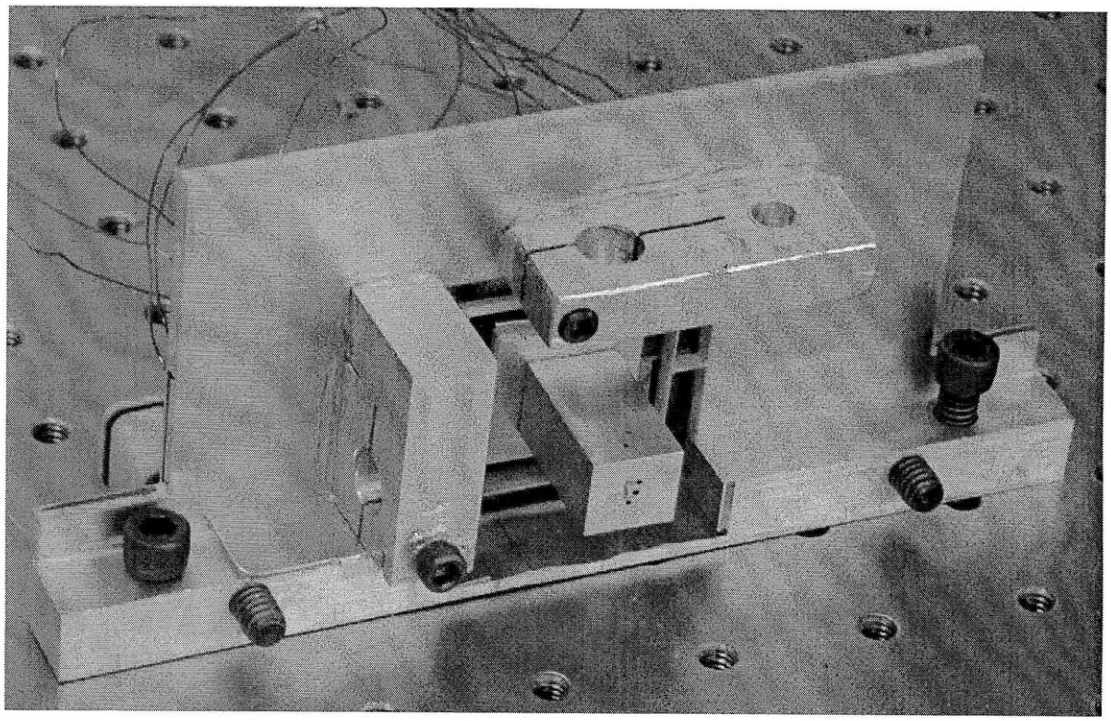

Figure C.10: Photograph of rear of test apparatus

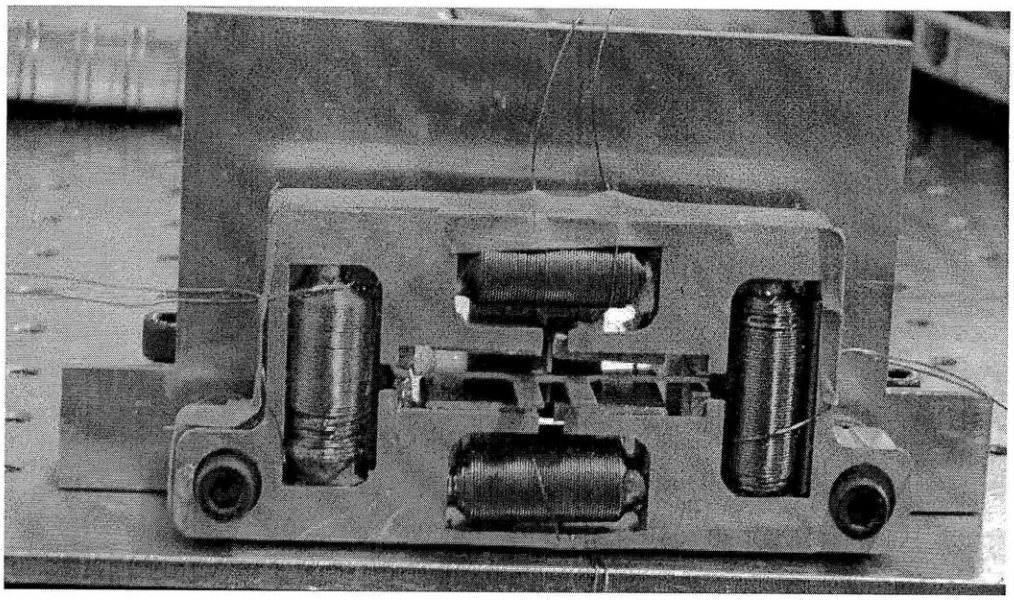

Figure C.11: Photograph of front of test apparatus

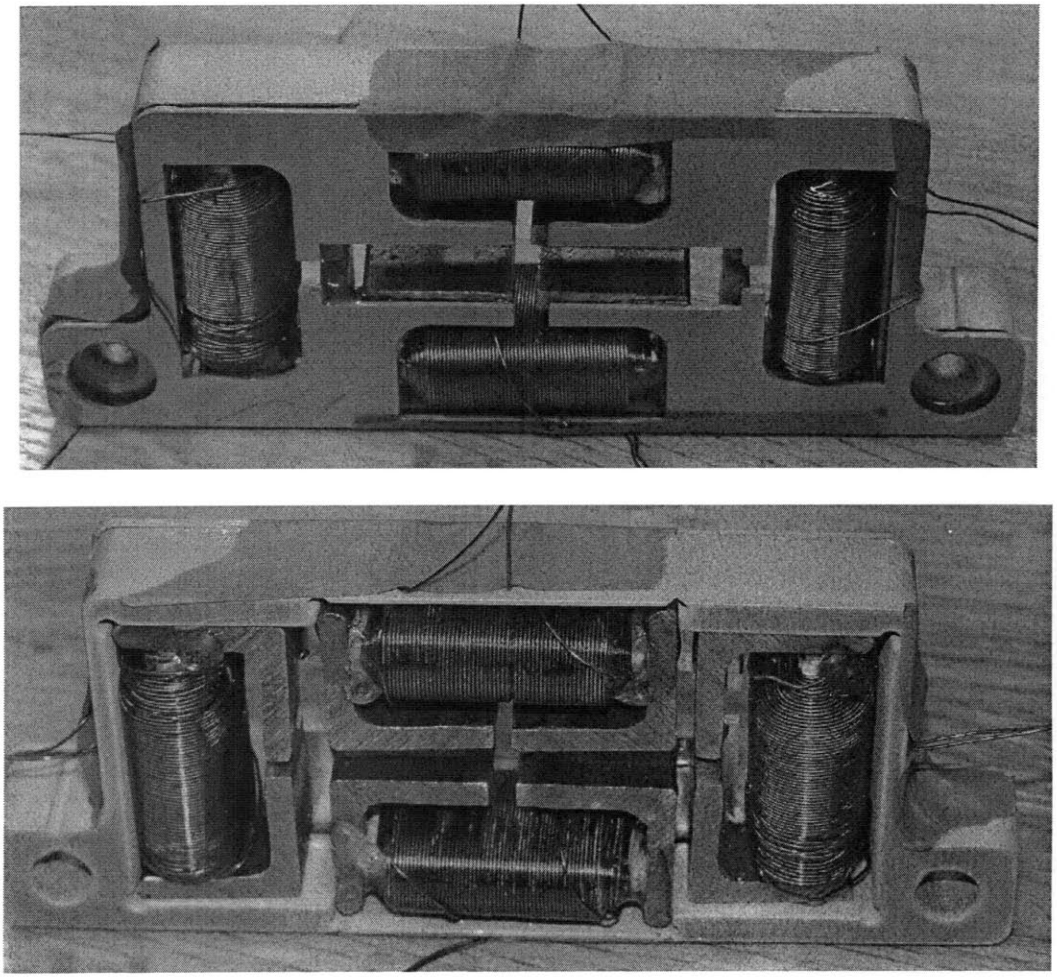

Figure C.12: Rear and front views of actuator prototype